Nanophotonic light trapping in solar cells

S. Mokkapati and K. R. Catchpole

Citation: J. Appl. Phys. **112**, 101101 (2012); doi: 10.1063/1.4747795
View online: http://dx.doi.org/10.1063/1.4747795
View Table of Contents: http://jap.aip.org/resource/1/JAPIAU/v112/i10
Published by the American Institute of Physics.

APPLIED PHYSICS REVIEWS—FOCUSED REVIEW

Nanophotonic light trapping in solar cells

S. Mokkapati[1] and K. R. Catchpole[2]
[1]*Department of Electronics Materials Engineering, Research School of Physics and Engineering, Australian National University, Canberra ACT-0200, Australia*
[2]*Center for Sustainable Energy Systems, Australain National University, Canberra ACT-0200, Australia*

(Received 17 April 2012; accepted 8 August 2012; published online 19 November 2012)

Nanophotonic light trapping for solar cells is an exciting field that has seen exponential growth in the last few years. There has been a growing appreciation for solar energy as a major solution to the world's energy problems, and the need to reduce materials costs by the use of thinner solar cells. At the same time, we have the newly developed ability to fabricate controlled structures on the nanoscale quickly and cheaply, and the computational power to optimize the structures and extract physical insights. In this paper, we review the theory of nanophotonic light trapping, with experimental examples given where possible. We focus particularly on periodic structures, since this is where physical understanding is most developed, and where theory and experiment can be most directly compared. We also provide a discussion on the parasitic losses and electrical effects that need to be considered when designing nanophotonic solar cells. © *2012 American Institute of Physics*. [http://dx.doi.org/10.1063/1.4747795]

TABLE OF CONTENTS

I. INTRODUCTION

Worldwide installed capacity of solar photovoltaic (PV) power has escalated from 1.3 GW in 2001 to 22.9 GW in 2009 and 35 GW in 2010 (Ref. 1) and has had an average growth rate of 40% over the last 5 years. Given that earth receives more energy from Sun in one day (10^{21} J) than is used by the world population in one year, PV contribution to the world energy has vast potential. Currently, the cost per Watt of power generated from PV is substantially higher than the current costs of power generated using conventional fossil fuels. Cost of power generation from PV needs to be reduced approximately by a factor of 2-3 (exact values depend on local solar insolation and electricity costs) to be comparable to that generated from conventional sources.

Currently, 80%–90% of the PV market is based on crystalline Si (c-Si) solar cells.[2] Si is the third most abundant element on Earth and has a near ideal band gap energy for maximizing the efficiency of a single junction solar cell. Si fabrication techniques developed by the microelectronics industry have played a critical role in the development of current c-Si solar cell technology. c-Si solar cells have now exceeded efficiency of 25% in the laboratory, and silicon modules have reached an efficiency of over 22%.[3]

High purity Si used in the fabrication of conventional c-Si solar cells requires expensive and energy intensive refining of the Si feedstock. Materials costs account for ~40% of the total cost of a typical c-Si PV module. Only 25% of the total costs are spent on actual cell fabrication. The rest is the module fabrication cost. An effective approach to reducing

the cost per watt of PV generated electricity would be to design and fabricate high efficiency solar cells based on thin active layers. Conventional c-Si solar cells are fabricated from 180–300 μm thick Si wafers. Fabricating thin film solar cells with an active layer thickness of hundreds of nanometers to few microns would reduce the material usage by a factor of 100. In addition to reduced materials usage, thin film solar cells also have the advantage of reduced carrier collection lengths. The photo-generated carriers in the cell should reach the external contacts before they recombine in order to generate electric current. The distance travelled by the carriers before recombination is called carrier diffusion length. For efficient collection of photo-generated carriers, the carrier diffusion length in the active material should be a few times larger than the thickness of the active layer. Reduced thicknesses facilitate the use of lower quality active material (material with lower carrier diffusion lengths) for the cell fabrication, further reducing the material and deposition costs.

Currently, CdTe (cadmium Telluride) holds the major share in thin film PV market. However, Tellurium is a rare material and might not be a suitable candidate to provide a significant fraction of the world's projected energy needs in the future. Si based thin-film technologies like a-Si:H (hydrogenated amorphous Si), polycrystalline Si and tandem microcrystalline Si, a-Si:H solar cell technologies are currently under intense investigation. Other potential candidate materials are organics and earth-abundant inorganic semiconductors such as copper-zinc-tin-sulphur (CZTS), CuO, and FeS_2.

A thin active layer, however, compromises the optical absorption in the solar cell. Figure 1 shows the spectral irradiance (in W/m^2/nm) on earth's surface for the AM1.5g solar spectrum, and the irradiance absorbed by a 2 μm thick Si layer, neglecting reflection losses (i.e., assuming a perfect anti-reflection coating on the front surface). As can be seen from Figure 1, for wavelengths greater than 500 nm, not all of the incident photons are absorbed in the Si layer. Part of the incident energy is lost because of transmission of light through the Si layer. These transmission losses are more significant in the long wavelength region, 700 nm–1180 nm, closer to the band-edge of Si. The transmission losses can be reduced by "folding" light multiple times into the absorbing region of the solar cell, thereby increasing the optical path length of light and hence the probability of its absorption inside the solar cell. This process is known as light trapping. By employing light trapping in a solar cell, the "optical thickness" of the active layer is increased several times while keeping its physical thickness unaltered. The ratio of the optical thickness to the physical thickness, i.e., the ratio of the path length travelled by photons inside the cell in the presence of light trapping to that with no light trapping, is known as the path length enhancement. This is an important parameter that enables quantitative comparison of different light trapping techniques.

Light trapping is achieved by modifying the surface of the solar cell to enhance the probability of total internal reflection. By doing so, light gets reflected back into the active volume several times. Figure 2 shows a glass slide with a light trapping pattern imprinted on its surface. The outline of the pattern can be seen clearly on the surface of the slide. When light hits the glass-air interface, it is reflected back completely into glass and cannot escape through the surface. Light can only escape the glass slide from its edges, making the edges colorful, as can be seen in the picture.

The best known technique for texturing the surface of a Si wafer is to form upright or inverted pyramids[4–8] or random textures.[9] This is the most widely used light trapping technique employed in industry. These pyramids have dimensions of the order of 1–10 μm. However, this approach is not suitable for thin solar cells where the active region itself is only a few microns or even a few hundred nanometers thick.

Thin solar cells need wavelength scale (or nanophotonic) structures for achieving light trapping. Different approaches for nanophotonic light trapping include periodic semiconductor or dielectric structures (one dimensional (1D), single period or dual period two dimensional (2D) diffraction gratings and photonic crystals), plasmonic

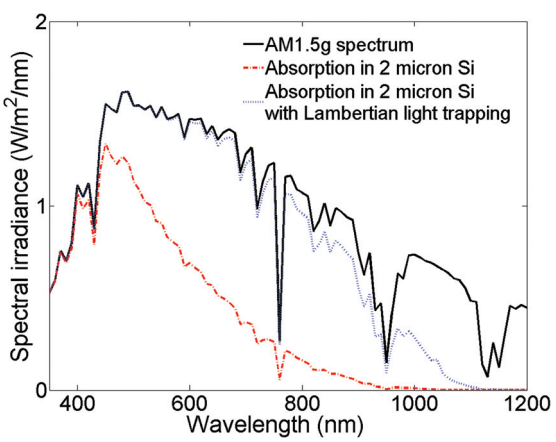

FIG. 1. The spectral irradiance on earth's surface, irradiance absorbed by a 2 μm thick Si layer and a 2 μm thick Si with Lambertian light trapping, neglecting the reflection losses.

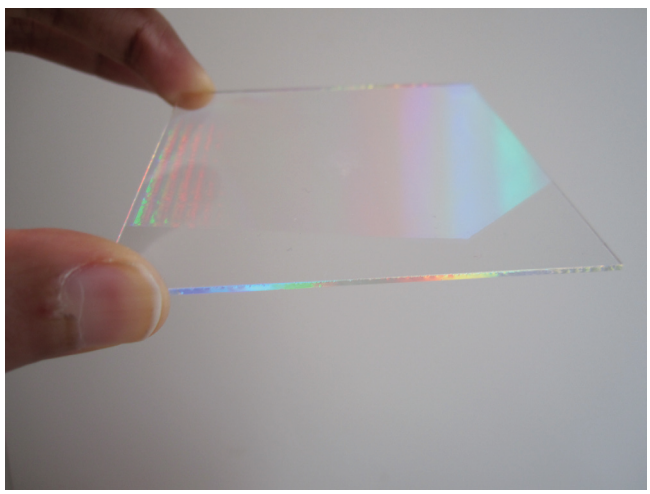

FIG. 2. A glass slide with an imprinted light trapping pattern on the surface. The pattern traps light effectively inside the glass, making it bounce back into the glass everytime it hits the glass-air interface. As a result, light is trapped and is directed to the edges of the glass slide, as can be seen here.

structures, and randomly structured semiconductor surfaces. The tremendous research efforts in the direction of designing best possible light trapping strategies for photovoltaics is evident in the fact that a search for publications in Scopus in 2001 for solar and light-trapping yields 24 publications, while the same search for 2011 yields 242 publications.

In this article, we provide a general introduction to nanophotonic light trapping in solar cells. We describe the potential for enhancement that they provide, including the work that has been done to date on the fundamental limits of these structures. We also describe the effect of losses and the measurement of light trapping, which are areas that have not received much attention to date. We give particular attention to periodic structures, for two important reasons. Periodic structures can provide high enhancements in their own right. In addition, there is very well developed theory for structures with very small or very large periods compared to the wavelength of incident light. Recent advances in numerical techniques for wavelength scale gratings help in gaining fundamental understanding of the mechanisms involved. Advances in processing technologies in recent times also make it possible to fabricate sub-wavelength scale structures with precisely controllable features and allow a direct comparison between theory and experiment for periodic structures. We also provide a brief discussion of the light trapping provided by other structures, and point to where more information on these topics can be found.

II. LAMBERTIAN LIGHT TRAPPING

Among the earliest work on the theory of light trapping was the derivation by Yablonovitch and Cody,[10] and independently by Göetzberger[11] of the light trapping achievable by an isotropically scattering (or Lambertian) surface. A Lambertian surface results in uniform brightness in a medium, irrespective of the angle of incidence of light on the medium, or the angle of observation. In this section, we will derive a simple expression for the path length enhancement that can be obtained in a solar cell using a Lambertian surface.

We follow the approach outlined in Refs. 8 and 11. The same result can be obtained using a statistical approach.[12] The approach used here is valid only in weakly absorbing limit, i.e., there is negligible absorption inside the structure or on the surface of the structure. Another important assumption is that the optical mode density in the structure is continuous and is unaffected by wave-optical effects. These conditions are satisfied if the optical thickness of the cell is much greater than $\lambda/2\,\mathrm{n}$, where λ is the wavelength of incident light and n is the refractive index of the material; and the surface texture is either random or has a period much larger than the wavelength, λ, of incident light.

It is assumed that the Lambertian surface has produced a uniform brightness (intensity per solid angle) of B inside the semiconductor. Any unit surface area of the semiconductor will have incident intensity $B\cos\theta$ per unit solid angle from rays oriented at an angle θ to its normal (see Figure 3). The proportion of light intensity incident on the surface that escapes from the surface, f, is the ratio of intensity resulting

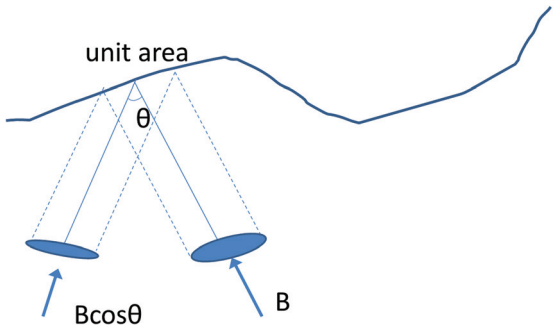

FIG. 3. Definition of angles associated with light incident on a perfectly randomizing surface. Adapted from Ref. 8.

from light rays within the loss cone (i.e., rays striking the surface at an angle smaller than the critical angle, θ_c) to the total intensity.

$$f = \frac{\int_0^{\theta_c} B\cos\theta\sin\theta d\theta}{\int_0^{\frac{\pi}{2}} B\cos\theta\sin\theta d\theta} = \sin^2\theta_c = \frac{1}{n^2}, \tag{1}$$

where n is the refractive index of the semiconductor.

In the absence of the Lambertian surface, normally incident light on a semiconductor substrate of thickness w would travel an average distance of w in one pass across the semiconductor. Because of the Lambertian scattering surface, light is scattered into the semiconductor at all angles with respect to the surface normal. A ray traversing at an angle θ with respect to the surface normal propagates a distance $w/\cos\theta$ in one pass across the semiconductor. Thus, the average path length for a single pass across the semiconductor for rays scattered by a Lambertian surface is

$$\frac{\int_0^{\frac{\pi}{2}} \frac{w}{\cos\theta}\cos\theta\sin\theta d\theta}{\int_0^{\frac{\pi}{2}} \cos\theta\sin\theta d\theta} = 2w. \tag{2}$$

The above two results can be used to calculate the average path length enhancement resulting from any Lambertian scheme. For a solar cell with front Lambertian surface and a rear reflector with reflectivity, R, the average path length is given by

$$2w(1-R) + 4wfR + 6wR(1-f)(1-R) + 8wf(1-f)R^2 + \ldots\ldots = \frac{2w(1+R)}{1-R(1-f)}. \tag{3}$$

For the limiting case of a perfect rear reflector, i.e., $R = 1$, the average path length becomes $4n^2w$; or the average path length enhancement with respect to a planar semiconductor of thickness w is $4n^2$. The same argument can be

followed for isotropic scattering in 2D rather than 3D, i.e., a plane normal to the scattering surface. For this case, by omitting $\sin\theta$ in the integrations in Eqs. (1) and (2) above, a path length enhancement of πn is obtained. A good overview of Lambertian and geometrical optics light trapping can be found in Brendel,[13] who also shows that for maximum current, the distribution of path lengths as well as the average path length is important.

As already mentioned, the above path length enhancement estimations are valid only for thick substrates with surface structures that can be described by geometrical optics. We will see in Secs. VII E and VIII D how wave-optics affect these results.

III. EFFECT OF LIGHT TRAPPING ON REQUIRED THICKNESS FOR STRONG AND WEAK ABSORBERS

The level of light trapping that can be achieved determines the thickness that is needed to achieve an adequate level of J_{sc}. Figure 4 shows the J_{sc} as a function of thickness for Si and GaAs, with either no light trapping (single pass absorption) or Lambertian light trapping. Note that the use of single pass absorption and Lambertian light trapping is not strictly valid for thicknesses below a few hundred nanometres, because waveguide effects need to be taken into account. Nevertheless, this simple calculation allows us to estimate the thickness required for a given semiconductor and level of light trapping. We can see from Figure 4 that for an indirect bandgap semiconductor like Si, light trapping decreases the thickness required to achieve a J_{sc} of $35\,mA/cm^2$ from about $40\,\mu m$ to about $2\,\mu m$. For a direct bandgap semiconductor such as GaAs, the thickness required to reach $28\,mA/cm^2$ is reduced from $1\,\mu m$ to 50 nm. The ability of light trapping to reduce the required thickness of direct bandgap semiconductors to tens of nanometres opens up the possibility of using a wide range of alternative materials for photovoltaics that have very low diffusion lengths, such as CuO and FeS_2.

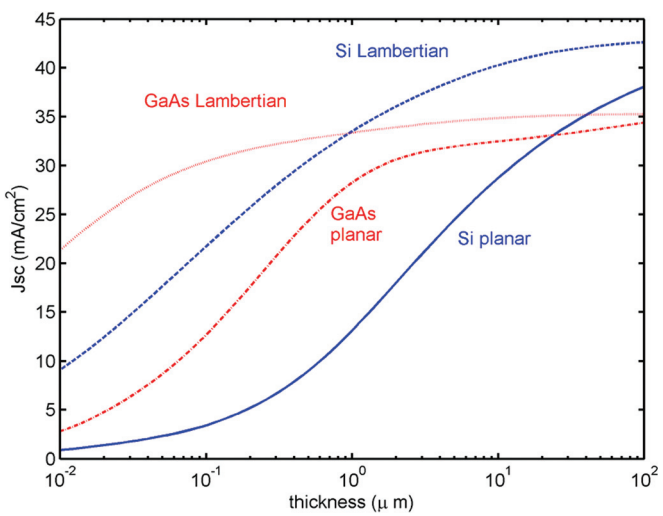

FIG. 4. J_{sc} vs. thickness for a direct bandgap semiconductor (GaAs) and an indirect bandgap semiconductor (Si), for either the planar case (assuming single pass absorption only) or Lambertian light trapping.

IV. EFFECT OF LOSSES

When considering the potential J_{sc} or path length enhancement in a solar cell, it is very important to also consider the effect of parasitic loss within the cell, due to, for example, absorption within a rear reflector.

To investigate this, we can use the analytical model for Lambertian light trapping given by Green,[14] valid for relatively thick cells that support a large number of waveguide modes. The total absorption in the cell, A_T, the absorption in the rear reflector, A_R and the absorption in the bulk region of a cell, A_B are then given by

$$A_T = \frac{(1-R_{ext})(1-R_bT^+T^-)}{1-R_fR_bT^+T^-}, \tag{4}$$

$$A_R = \frac{(1-R_{ext})(1-R_bT^+)}{1-R_fR_bT^+T^-}, \tag{5}$$

$$A_B = A_T - A_R, \tag{6}$$

where R_{ext} is the external front reflectance, R_b is the internal rear reflectance, and R_f is the internal front reflectance. T^+ (T^-) is the fraction of downward (upward) light transmitted to the rear (front) surface, and expressions for these are given in Ref. 14.

In Figure 5, we set $R_{ext}=0$ and investigate the effect of loss at the rear reflector $(1-R_b)$ on the J_{sc} and path length

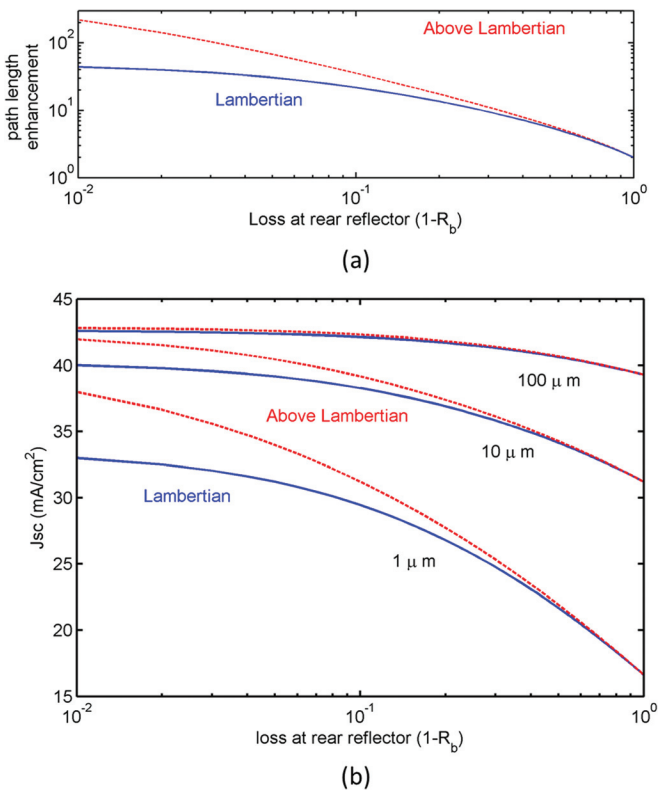

FIG. 5. (a) Path length enhancement vs. loss at the rear reflector $(1-R_b)$. The blue solid line is for Lambertian light trapping ($R_f=1-1/n^2$), where n is the refractive index of silicon. The red dashed line is for an internal front reflectivity loss with 10% of the value for Lambertian light trapping, i.e., $R_f=1-0.1/n^2$. (b) J_{sc} vs. loss at the rear reflector $(1-R_b)$. The blue solid lines are for Lambertian light trapping, while the red dashed lines are for above Lambertian light trapping, as in (a). Three thicknesses of silicon are shown: $100\,\mu m$, $10\,\mu m$, and $1\,\mu m$.

enhancement, for different values of thickness and R_f. The effect of parasitic loss at the rear reflector on the path length enhancement is plotted in Figure 5(a), and can be obtained from the long wavelength limit of Eqs. (4)–(6) or directly from Eq. (3). Figure 5(a) shows the path length enhancement vs. rear reflector loss for an internal front reflectivity corresponding to Lambertian light trapping, $R_f = 1 - 1/n^2$ (blue solid line), and for an example of above Lambertian light trapping (red dashed line). The above Lambertian case corresponds to an internal front reflectivity loss of 10% of the Lambertian value, i.e., $R_f = 1 - 0.1/n^2$. We can see that if the loss at the rear reflector is very low (1%), the path length enhancement for the Lambertian case is close to the ideal value of $4n^2 \approx 50$. However, once the rear loss has reached 5%, the enhancement is reduced to around 30. The drop is more severe for above Lambertian light trapping, with a decrease from a value of around 200 for a 1% rear loss to 70 for a 5% loss.

More important than the effect on path length enhancement is the effect on J_{sc}. Figure 5(b) shows J_{sc} as a function of loss at the rear reflector for the two different light trapping cases used in Figure 5(a), and for three different solar cell thicknesses. We can see that for a 100 μm thick silicon solar cell, there is no significant benefit in above Lambertian light trapping, regardless of the loss at the rear reflector. For a 1 μm thick cell, there is a potential current gain of 5 mA/cm^2 for above Lambertian light trapping, but this requires a rear reflector loss of 1%. For a rear loss of 5%, the potential current gain is reduced to 3 mA/cm^2.

Thus, above Lambertian light trapping can only have a signficant J_{sc} benefit if parasitic losses are very low, i.e., less than a few percent. This would seem to preclude the use of metals and heavily doped semiconductors in the cell design, unless the amounts used are very small.

V. ELECTRICAL EFFECTS

The inclusion of light trapping reduces the optimum thickness of cells, as this allows high currents to be maintained but with lower bulk recombination. However, it is also important to consider the effect of surface recombination, which becomes relatively more important as cell thickness decreases. For 1 μm thick silicon cells, the maximum efficiency with no surface recombination is 24%. For a low level of surface recombination ($J_0 = 25$ fA/cm^2), the efficiency is reduced to 20%; and for relatively high surface recombination, the efficiency becomes 16%.[15] The lesson here is that for ultra-thin device concepts, an estimate of the effect of surface recombination needs to be made before doing detailed optical modeling.

Light trapping, or equivalently (because of the reciprocity of light) light extraction, is also very important in reaching the ultimate limits on the open-circuit voltage for solar cells. This is because the efficiency of photon re-emission is a measure of how ideally a solar cell behaves.[16,17] At open circuit, the emitted radiation and absorbed radiation must exactly balance the incoming radiation. Hence, the lower the non-radiative recombination, the higher the radiative recombination. The effect of photon emission efficiency, η_{ext}, on open circuit voltage can be seen from Eq. (7), derived by Ross,[18] and discussed further in Refs. 16, 17, and 19:

$$V_{oc} = V_{oc-ideal} - (kT/q)\ln(\eta_{ext}). \quad (7)$$

For a thin cell in the geometric optics limit and no losses, $\eta_{ext} = I\eta_{int}/4n^2$, where I is the light concentration factor and η_{int} is the internal photon emission efficiency. Thus, the inclusion of ideal Lambertian light trapping (i.e., $I = 4n^2$) can increase the open-circuit voltage by about (kT/q) $\ln(50) = 100$ mV, using the room temperature thermal voltage of 26 mV for kT/q. In practice, the effect has been lower to date. Trupke *et al*. have estimated an increase in the photo-emitted current from Si wafers of a factor of 7 due to pyramid textures.[20] This would correspond to an increase in voltage of 50 mV. For high quality GaAs cells, surface texturing is not necessary, although a good mirror is required to achieve the open-circuit voltage benefit that light extraction gives.[16] For these cells, the internal quantum efficiency (IQE) is so high ($\gg$90%) that photon-recycling gives emitted photons many chances to escape, much like surface texturing does for cells with lower internal quantum efficiencies.

For practical applications, the electrical performance of the solar cell in the presence of a grating or photonic crystal structure also needs be considered. If a grating is fabricated in the active layer of the solar cells, it tends to lead to increased surface recombination. Additionally, if the active layer is deposited on a substrate with a grating structure, steep features can make subsequent deposition of high quality material difficult (see, e.g., Ref. 21). Currently, methods for evaluating the overall cell performance by integrating electrical and optical characteristics of the cell are being developed. Li *et al*. have developed a multi-dimensional optical and electrical model for solar cells and achieved good agreement with experimental results for thin GaAs solar cells.[22] They also showed that including electrical effects is necessary to get accurate results when modelling materials with low carrier mobility, such as amorphous silicon.[23]

VI. MEASURING LIGHT TRAPPING

The most common method to evaluate light trapping for nanophotonic structures is to calculate the enhancement factor, i.e., the photocurrent at long wavelengths divided by the photocurrent for a reference sample. In the literature, this is sometimes known as Z. This is then compared with the $4n^2$ value. However, care must be taken with this approach, as the enhancement obtained is very sensitive to the low, and often noisy, long wavelength photocurrent data of the reference sample.

An alternative method is to measure the J_{sc} for the test sample and compare it to the J_{sc} for a reference sample. These values can also be obtained from measurements of the external quantum efficiency as a function of wavelength for each sample, which are then integrated over the photon flux for the solar spectrum to obtain J_{sc}. In this case, it is important to provide the enhancement that would have been obtained for a benchmark case, such as Lambertian light

trapping, since the enhancement in J_{sc} that is achievable depends strongly on the solar cell thickness.

A less widely used method is the extended spectral analysis of IQE, introduced by Basore.[24] This involves plotting the inverse IQE against the inverse absorption co-efficient. By making use of an optical model, the light trapping enhancement factor Z can be obtained. This method provides a more accurate result, since Z is obtained from measurements over a range of wavelengths, rather than at a single wavelength. An example of the use of this analysis for a plasmonic solar cell can be found in Ref. 25. Note that the optical model was developed for wafers and would need to be modified for thin cells.

In the development of light trapping structures for solar cells, it is often an advantage to be able to assess a light trapping structure without the need to make a complete solar cell. Absorptance measurements on their own are not particularly useful, because they do not separate absorption that generates an electron-hole pair from parasitic absorption. Trupke *et al*. have presented a method for obtaining the useful absorptance and the light trapping enhancement factor Z from measurements of luminescence.[26] The measurements were performed using electroluminescence but could be generalized to photoluminescence. The method involves obtaining the absorptance due to band-to-band transitions from the luminescence spectrum, making use of the generalized Planck's law. This is then fitted to a Lambertian model in the long wavelength region of the spectrum to obtain Z.

VII. PERIODIC LIGHT TRAPPING STRUCTURES

One, two, or three dimensional (1D, 2D, or 3D) periodic dielectric structures or gratings have the potential to enhance the optical absorption of solar cells in several ways. Figure 6 shows a schematic representation of gratings used in different forms to enhance the solar cell performance. Optimised 1D dielectric gratings or Bragg stacks can be used as back reflectors that double the path length of light in the active volume of a solar cell (Figure 6(a)). Single period or bi-periodic dielectric structures can be used for reducing the reflection from the illuminated surface of the solar cell or for trapping light inside the active volume of the cell (Figure 6(b)). Light trapping can be achieved by either coupling light into the guided modes of the active region (if the active region supports only a few waveguided modes) or by coupling light into diffraction modes that propagate outside the loss cone in the active volume (when the active region is relatively thick and supports a continuous density of photonic modes). In tandem solar cells, 3D periodic dielectric structures or photonic crystals can be used as highly efficient omnidirectional reflectors[27] (Figure 6(c)). Alternatively, the active volume itself can be patterned in 3D to confine light and increase the absorption of long wavelength light[28–33] (Figure 6(d)). Several gratings can be used in conjunction to each other to achieve one or more of the above mentioned effects simultaneously.

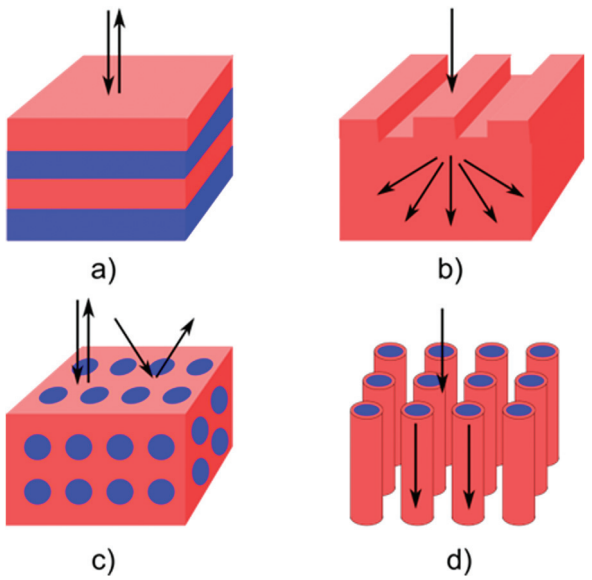

FIG. 6. Schematic illustration of periodic dielectric structures used for enhancing solar cell performance: (a) 1D (Bragg) stacks used as back reflectors, (b) 2D gratings, used for anti-reflection and/or light trapping (c), and (d) 3D photonic crystals, which are highly effective as omnidirectional reflectors or trap light by a waveguiding effect. Reproduced with permission from Catchpole *et al*., MRS Bull. **36**, 461 (2009). Copyright © 2011 Cambridge University Press.

A. Gratings for back-reflectors and anti-reflection

A Bragg stack or a distributed Bragg reflector (DBR) is the simplest (1D) form of a grating. Light reflected from different layers of the stack interfere constructively or destructively leading to high reflectance or transmittance. Bragg stacks are efficient only for a narrow wavelength range and are also very sensitive to the incidence angle. Their wavelength selective nature makes them unsuitable for use as broadband anti-reflective layers for solar cells. However, they have been used as low loss, efficient rear reflectors in thin solar cells to efficiently reflect a narrow band of light transmitted through the solar cell.

2D dielectric gratings with characteristic features smaller than that of the wavelength of incident light act as efficient anti-reflection layers.[34–50] Figure 7(a) shows the schematic of a 2D grating with periodicity, *d*, in x- and y-directions. The periodicity of the grating imposes constraints on the direction of propagation of light in air and in the absorbing medium. Only plane-waves whose in-plane wavevectors satisfy the relation

$$\vec{k} = \vec{k_0} + G_{m_1,m_2} \tag{8}$$

can propagate. Here, $\vec{k_0}$ is the in-plane wavevector of incident light and G_{m_1,m_2} is the grating vector defined as

$$G_{m_1,m_2} = m_1 \frac{2\pi}{d}\vec{x} + m_2 \frac{2\pi}{d}\vec{y}, \tag{9}$$

where m_1 and m_2 are integers are supported. The wavevectors for the diffraction modes are shown (as green dots) in wavevector space or k-space in Figure 7(b). The allowed modes are separated from each other by $\frac{2\pi}{d}$. In addition, propagating modes in air and the absorbing medium are bounded by circles in k-space with radii $\frac{2\pi}{\lambda}$ and $n\frac{2\pi}{\lambda}$, respectively, where λ is the wavelength of incident light in air and n is the

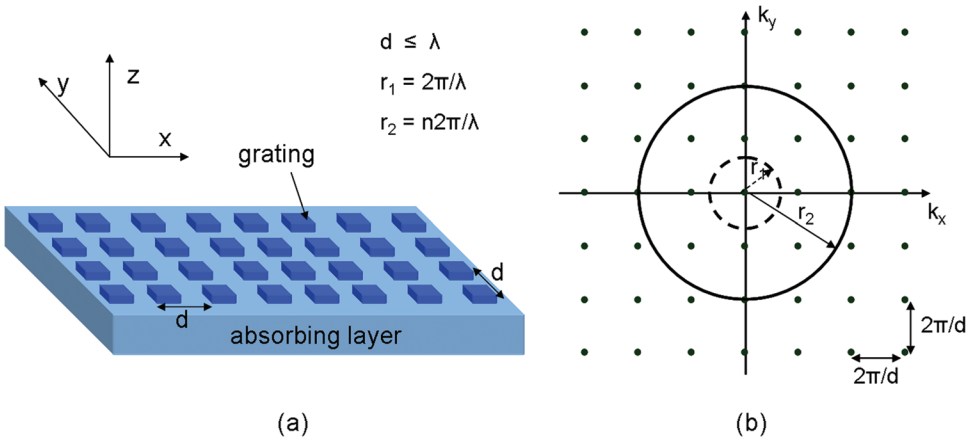

FIG. 7. (a) Schematic of a 2D grating structure with periodicity d. (b) Allowed diffraction modes in k-space or reciprocal space. Circles with radii r_1 and r_2 represent the maximum allowed k vectors for propagating modes in air and the absorbing medium, respectively. n is the refractive index of the absorbing medium.

refractive index of the absorbing medium. The dots inside the circles represent the wavevectors for propagating plane wave modes to which incident plane waves can couple.

Gratings can provide anti-reflection by two mechanisms. For gratings with periodicity $d \leq \lambda$, incident plane waves can couple to only one propagating diffraction mode in air, the principal diffraction order or the 0th diffraction order. Since the absorbing layer has higher refractive index than air, for periods (d) slightly smaller than the wavelength of incident light (λ), incident light can couple to a larger number of propagating diffraction modes inside the absorbing medium (dots that lie inside the circle of radius r_2). Since incident light can couple to only one diffraction mode in air, but to a larger number of modes inside the absorbing material, most of the incident light is coupled into the solar cell and hence such gratings act as efficient anti-reflection layers (and may also provide light trapping due to coupling of light to higher order diffraction modes).

For gratings with periods much smaller than the wavelength ($d \ll \lambda$), only the zeroth diffraction order is present in both air and in the substrate. Such gratings cannot provide light trapping because they do not change the direction of the incident light. However, subwavelength period gratings can reduce reflection, since the grating can provide impedance matching. Impedance matching is matching the in-plane components of the wave vectors between the grating modes and diffraction modes in air and substrate. Grating modes refer to the electromagnetic modes that propagate inside the grating. Each grating mode is characterized by an effective refractive index, n^{eff}. The grating modes for a 1D lamellar grating (schematic in Figure 8(a)) can be obtained by solving the photonic crystal equation (Eq. (10)),[51,52] since a 1D lamellar grating is essentially a 1D photonic crystal.

$$f(n^{eff}) = \cos(k_{xr}L_r)\cos(k_{xg}L_g) - \frac{1}{2}\left(\tau\frac{k_{xr}}{k_{xg}} + \frac{1}{\tau}\frac{k_{xg}}{k_{xr}}\right) \times \sin(k_{xr}L_r)\sin(k_{xg}L_g) = \cos(k_{x0}L), \quad (10)$$

where

$$k_{x0} = k_0 \sin(\theta_{in}) = \frac{2\pi}{\lambda} n_a \sin(\theta_{in})$$

is the x component of the wave vector of the incident wave and

$$k_{xi} = k_0[n_i^2 - (n^{eff})^2]^{1/2}, \quad i = r, g$$

are the x components of the wave vectors in the ridges and grooves of the grating, respectively. L is the period of the grating, L_r is the width of the ridges, and L_g is the width of the grooves.

$\tau = 1$ when the electric field is perpendicular to the direction of propagation (TE polarization) and $\tau = \frac{n_r^2}{n_g^2}$ when the electric field is perpendicular to the direction of propagation (TM polarization). n_r and n_g are the refractive indices of the ridges and grooves, respectively. n_a is the refractive index of the incident medium, and n_s is the refractive index of the substrate.

For a bi-periodic grating (Figure 8(b)), an expression similar to the 1D photonic crystal equation (Eq. (10)) does not exist. It has been shown that the effective index method can be used to calculate the effective indices of the grating

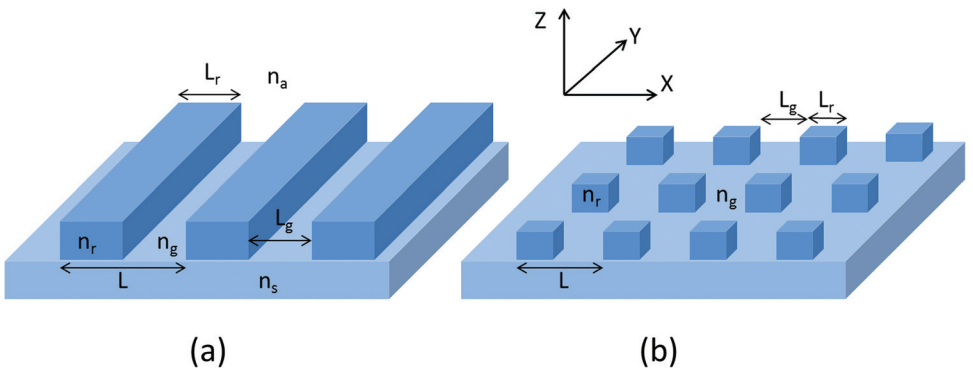

FIG. 8. Schematic showing the parameters of (a) 1D lamellar grating and (b) 2D pillar grating used for illustrating the methods of determining the grating modes (the photonic crystal equation for (a) and the effective index method for (b)).

modes for 2D sub-wavelength scale gratings.[53] Detailed analysis can be found in Ref. 54.

A large mismatch between the in-plane component of the wave vector of incident light and that of the mode propagating in the substrate (poor impedance matching) leads to high reflectance from a high index substrate. With a diffraction grating on the surface of the substrate with $n_s = n_r$ and $n_a = n_g$, the effective refractive index, n^{eff} of the grating mode satisfies $n_a < n^{eff} < n_s$. n^{eff} between n_a and n_s leads to better coupling or efficient power transfer between the incident mode and the grating mode and between the grating mode and the diffraction mode in the substrate, in effect reducing the reflection from the substrate surface. Even better power transfer or anti-reflection can be obtained by designing the grating such that n^{eff} varies gradually and continuously between n_a and n_s from top of the grating to its base. n^{eff} can be gradually varied by choosing a tapered profile for the unit cell of the grating. Such a grating can be treated as a layered structure with several gratings of the same period (L) but continuously varying L_r and L_g (L_r decreasing from the base to the top of the grating and L_g increasing from the base to the top of the grating).

An example of sub-wavelength scale periodic structure that acts as an efficient anti-reflection layer is the moth eye structure (Figure 9–reproduced from Ref. 36). Such structure can be treated as a homogeneous medium that has a gradually changing refractive index between that of air and the semiconductor active layer; hence it provides better impedance matching and couples light efficiently into the semiconductor, with minimal reflection losses. Effective medium theory is widely used for the analysis of single period and bi-periodic subwavelength scale periodic dielectric structures.[37,50,55–58] RCWA (rigorous coupled wave analysis) simulations have also been widely used to optimise such structures for anti-reflection layers.[59]

Subwavelength scale periodic dielectric structures for anti-reflection layers have been fabricated using techniques like electron beam lithography followed by reactive ion etching,[36] fast atom beam etching through alumina templates.[60] Cheap and large area fabrication techniques like embossing in a sol-gel,[44,49] or using spin coated or self-assembled dielectric spheres as etch patterns/masks[38,39,48] have also been developed for fabrication of subwavelength scale gratings that could be employed as anti-reflection layers on solar cells.

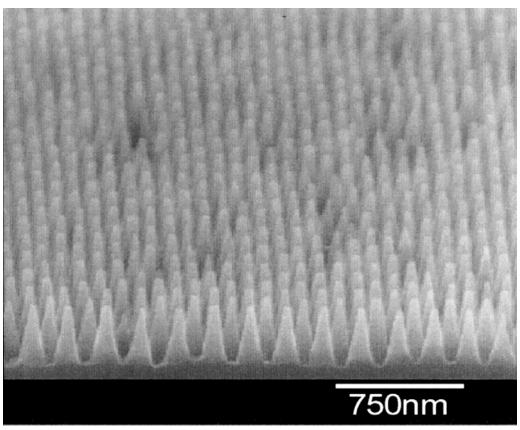

FIG. 9. Moth eye structure fabricated using electron beam lithography and reactive ion etching for application as an anti-reflection layer. Reproduced with permission from Sai *et al.*, Prog. Photovoltaics **15**(5), 415 (2007). Copyright © 2007 John Wiley & Sons Ltd.

Nano-cone arrays on a-Si:H thin film cells have demonstrated enhanced absorption because of anti-reflection property of the arrays.[48] 25% enhancement in efficiency of 2 μm thick c-Si solar cell has been achieved by incorporating anti-reflection gratings fabricated by interference lithography. An anti-reflection grating reduced the reflectance of the cell to less than 10% in 300–1200 nm range.[42] external quantum efficiency (EQE) enhancement of 3.5% was achieved in organic solar cells by employing a moth-eye anti-reflection structure.[45]

B. Gratings for light trapping

Two-dimensional (2D) gratings with periods larger than that of the incident wavelength (in the medium) support higher order diffraction modes that propagate at an angle with respect to the surface normal. The propagation angle for a diffraction order can be calculated using the grating equation (Eq. (11))

$$n_1 \sin\theta_{1m} = n_2 \sin\theta_{2m} = \frac{m\lambda}{d}, \tag{11}$$

where θ is the angle of propagation in each medium, m is the grating order (an integer), λ is the wavelength of light, and d is the period of the grating. Light trapping can be achieved by designing the gratings such that most of the light incident on the gratings is coupled to diffraction orders propagating outside the escape cone in the active volume of the solar cell. The effect of grating period on sensitivity to wavelength of incident light is schematically illustrated in Figure 10. Figures 10(a) and 10(b) show the allowed diffraction modes in k-space for a 2D grating with period d_1 and d_2, respectively, such that $d_1 > d_2$. The red and blue circles represent the range of k-vectors for propagating modes inside the absorber layer for light of wavelength λ_1 and λ_2, respectively, such that $\lambda_1 > \lambda_2$. The dots inside these circles represent propagating diffraction modes for the corresponding wavelength. For large period gratings (Figure 10(a)), the relative change in the number of propagating diffraction modes is very small compared to the relative change in the number of propagating diffraction modes for small period gratings (Figure 10(b)) when the wavelength of incident light is varied. The relatively small change in the number of propagating diffraction modes for large period gratings makes them less wavelength sensitive than small period gratings.

Key advantages of relatively large period diffraction gratings is that they are less wavelength sensitive, which is important in achieving light trapping for thin films which are weakly absorbing over a broad wavelength range.

The earliest work on gratings for solar cells was performed by Sheng *et al.*,[61] who demonstrated through numerical calculations that the short-circuit current density of a 500 nm thick a-Si:H solar cell could be increased by 2 mA/cm^2 using 1D patterned Ag back reflectors and by 3.5–4 mA/cm^2 using 2D gratings.[62] Recently, a great deal of

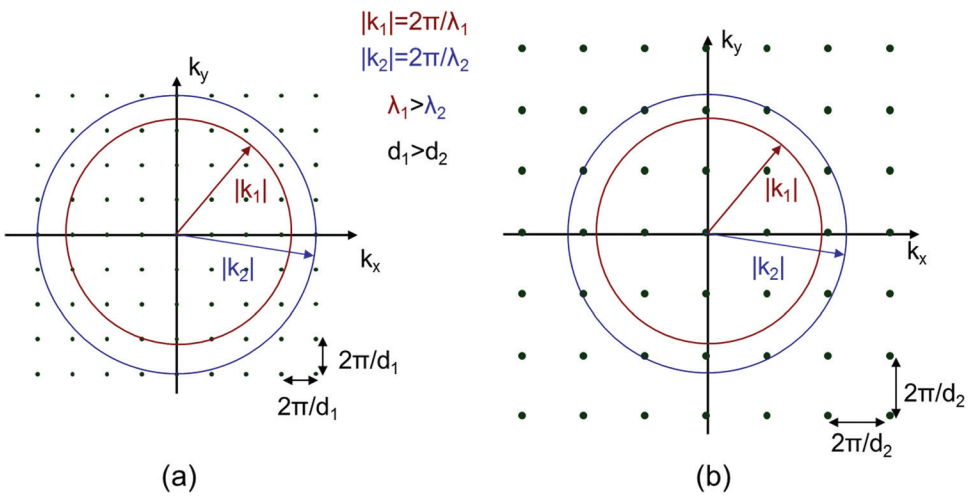

FIG. 10. (a) and (b) Schematic demonstration of the effect of grating period, d on the wavelength dependence of the grating performance. The dots represent the allowed diffraction modes in k-space (reciprocal space) for normal incidence. The areas bounded by the circles represent the allowed in-plane k vectors for the propagating modes supported by the medium. The radii of the circles are $|k_1|$ or $|k_2|$.

work has been done to investigate periodic structures for light trapping, both numerically and experimentally. In order to compare the performance of some of the different structures that have been investigated, the short-circuit current density that has been obtained for cells based on crystalline silicon has been plotted in Figure 11. The short circuit current densities expected for single pass absorption, with an ideal rear reflector and with Lambertian light trapping, are shown for reference. A perfect anti-reflection coating is assumed for these cases. It is important to note that the performance of a given light trapping technique cannot be gauged by comparing only J_{sc} from a solar cell with light trapping to that expected from a solar cell of the same thickness with Lambertian light trapping. The enhancement in J_{sc} also depends on the electrical performance of the reference cell (original cell without any light trapping) and this should be taken into account for a fair comparison.

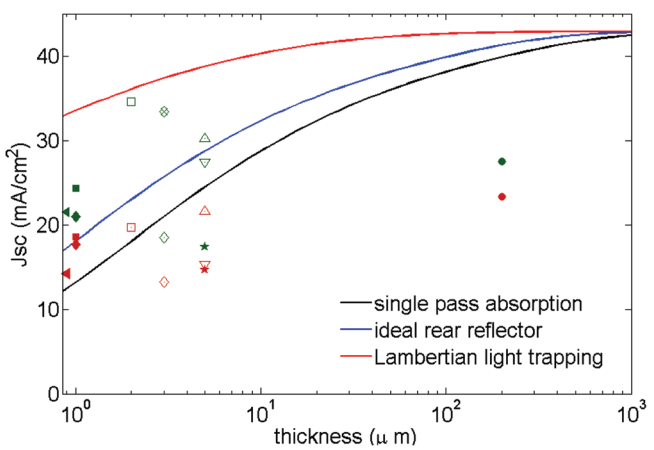

FIG. 11. Effect of incorporating wavelength scale diffraction gratings on the short circuit current density of a crystalline silicon solar cell. Ideal (theoretically evaluated) current densities expected from a solar cell for single pass, with an ideal rear reflector and with a Lambertian light trapping are also shown for reference. A perfect anti-reflection layer is assumed for these cases. The symbols in red correspond to the reference solar cell and the same symbol in green corresponds to the case where gratings are used to enhance the solar cell performance. Open symbols correspond to numerical results (up-triangles,[64] down triangles,[64] diamonds and crossed diamond,[68] and squares[69]) and filled symbols correspond to experimental results (circles,[62] stars,[66] triangles,[74] squares,[71] and diamonds[72]).

Enhanced solar cell performance has been predicted and demonstrated by using optimized Bragg stacks as rear reflectors in conjunction with 2D/3D dielectric gratings.[27,62–67] Zeng *et al.*[62] have demonstrated an increase in short circuit current density from 23.3 mA/cm^2 to 27.5 mA/cm^2 in wafer based c-Si solar cells by employing a rear grating and a Si_3N_4/Si DBR. These short circuit current densities are represented in Figure 11 as circles. The red circle is the reference case and the green circle is the cell with the rear grating and the DBR. The same research group has demonstrated a 8.82% power conversion efficiency in 5 μm thick microcrystalline Si solar cells by employing a grating and a wavy DBR on the rear of the cell.[66] These values are represented as stars (red for reference and green for the cell with gratings incorporated) in Figure 11. The power conversion efficiency in a reference cell was 7.68%. Mutitu *et al.*[64] have demonstrated through numerical studies that the short circuit current density resulting from photons in the 400–1100 nm range can be enhanced by 78.5% with respect to a bare 5 μm thick c-Si cell by incorporating a Si/SiO_2 DBR with a binary grating etched into it on the rear of the cell and an optimized anti-reflection (AR) coating on the front surface (represented by open down triangles, red for reference and green for the enhanced solar cell in Figure 11). The short circuit current density enhancement can further be increased to 97.2% by incorporating a triangular grating below the AR coating on the front surface of the cell (represented by open up triangles, red for reference and green for the enhanced solar cell in Figure 11). Chong *et al.*[68] have demonstrated through numerical studies that by using blazed TiO_2 gratings on the rear of a 3 μm thick c-Si solar cell, the short circuit current density can be increase from 13.2 mA/cm^2 to 18.5 mA/cm^2 (represented as open diamonds in Figure 11, red for reference and green for the cell with gratings) and by using Si skewed pyramid gratings on the front surface, J_{sc} can be increased to 33.4 mA/cm^2, which is 91% of the J_{sc} expected from an ideal Lambertian surface (value represented as crossed diamond in green in Figure 11). Wang *et al.*[69] have shown through numerical studies that by incorporating periodic nano-cone structures on the front for anti-reflection and on the rear for light trapping, the short circuit current density from a 2 μm thick c-Si cell can be increased from 19.7 mA/cm^2 to 34.6 mA/cm^2

(represented as open squares in Figure 11, red for reference and green for the cell with gratings).

Enhanced solar cell performance has also been predicted for periodic metallic gratings, and the design considerations for metallic gratings have been well established.[70] Sai *et al.*[71] have demonstrated that fabricating thin film solar cells on a patterned metallic substrate increases the short circuit current density from 18.6 mA/cm^2 to 24.3 mA/cm^2 for 1 μm thick μc-Si active layer (represented as filled squares in Figure 11, red for reference and green for the cell fabricated on periodically patterned substrate). Paetzold *et al.*[72] have experimentally demonstrated by depositing $\sim$1 μm thick μc-Si solar cells on periodically patterned metallic rear surface, the J_{sc} can be increased to 21.0 mA/cm^2, compared to 17.7 mA/cm^2 for a planar cell (represented as filled diamonds in Figure 11, red for reference and green for the cell with patterned rear reflector). Ferry *et al.*[73] have studied the effect of randomness of the patterned plasmonic back reflector on the performance of a-Si:H solar cell. It has also been reported that periodic photonic-plasmonic structures scatter light more efficiently than a randomly textured surface,[74] and the short circuit current density increased from 14.2 mA/cm^2 to 21.5 mA/cm^2 by incorporating a photonic-plasmonic back reflector into the design of a nc-Si solar cell with active region thickness $\sim$0.9 μm (represented as filled triangles in Figure 11). Some of the reports mentioned here, e.g.,[71–74] use both plasmonic effects and periodically patterned semiconductors to achieve light trapping.

In other notable work, Battaglia *et al.*[75] demonstrated that the efficiency of a-Si:H solar cells can be increased from 7.9% to 10.9% by fabricating the cells on substrates patterned with periodic nanocavities. Zhao *et al.*[67] studied 2 μm thick c-Si solar cells with an indium tin oxide (ITO) antireflection coating on the front and a diffraction grating with a DBR and an Ag reflector on the rear using RCWA. They predict that the absorption of the cell can be increased from 31% (of the incident AM1.5 spectrum) for a reference cell with just an ITO AR coating to 69% when a rear grating is used in conjunction with a 4 layer a-Si:H/ITO Bragg stack and a Ag mirror. The absorption can be increased further to 72% by using an 8 layer DBR. Numerical studies by Zhou *et al.*[63] have demonstrated enhanced photon absorption in a 500 nm thick a-Si:H absorber layer in the 600–775 nm wavelength range by employing a a-Si:H/ITO square lattice photonic crystal and a DBR with c-Si/SiO_2 layers or c-Si/ITO layers on the rear of the cell. Isabella *et al.*[76] demonstrated enhanced EQE in p (5 nm)-i (300 nm)-n (20 nm) a-Si: H solar cells deposited on modulated surface textured ZnO:Al. Haase and Stieberg[77] have predicted through simulations that the short circuit current density of a 1 μm thick c-Si solar cell can be increased by 18.7% using rectangular gratings and by 28.2% using 6 step blazed (asymmetric) gratings.

Diffraction gratings can be numerically modelled by methods such as RCWA[78,79] or finite difference time domain (FDTD) simulations. However, there is a wide parameter space over which the simulations need to be run, and the numerical results do not offer any physical insight into why a particular set of grating parameters should result in optimal performance. There are a few important cases of gratings where physical insight into the grating behaviour can be obtained using analytical techniques, which are described in Sec. VII C and D. These include rectangular gratings and pillar gratings (Sec. VII C, below) and large period gratings with arbitrary shape (Sec. VII D). The fundamental limit to the light trapping that can be achieved using diffraction gratings can also be analytically determined using statistical coupled mode theory (Sec. VII E).[80]

C. Understanding rectangular and pillar gratings

Rectangular gratings and pillar gratings are simple structures that are technologically important because they can be fabricated relatively easily. It has been shown that simplified modal analysis[52,81,82] can be used to predict the optimal parameters for rectangular gratings for coupling most of the incident light into diffraction orders propagating outside the loss cone.[54,83] The modal analysis also provides insight into the physical processes that dictate the optimal grating parameters and can be used to predict the parameters for the best performing rectangular gratings on a thin film solar cell without the need for extensive simulations.

Modal analysis divides the fields propagating in each region into different types of modes: the incident mode, the grating modes (modes propagating in the grating) and the reflected or transmitted diffracted modes. The number of allowed grating modes, their effective refractive indices, n^{eff} and the associated field distributions can be analytically determined using the photonic crystal equation, Eq. (10).

Figure 12 shows the diffuse transmittance for a rectangular Si grating on an infinite Si substrate, as a function of wavelength and grating height. It can be seen that there are periodic peaks in the diffuse transmittance, for a given wavelength.[83] The positions of these peaks can be accurately predicted by the interference of optical modes within the grating. When the period of the grating is such that only the 0th grating mode is excited, Fabry-Perot resonances inside the grating determine the efficiency of coupling between the grating mode and the diffracted modes. For a given wavelength λ, minimal light is coupled into the principal (0th) diffraction order when the grating height, h is such that

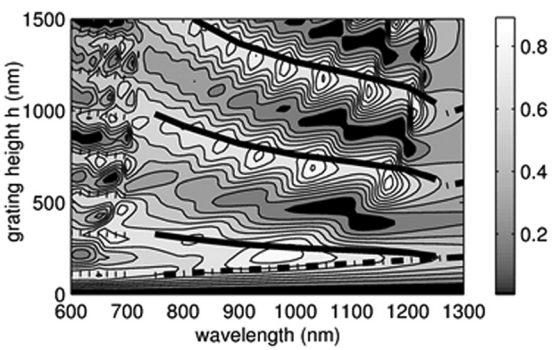

FIG. 12. Contour plot of diffuse transmittance vs wavelength and height for a rectangular Si grating on an infinite Si substrate with L = 650 nm calculated with RCWA. The lines show the maxima predicted with modal analysis. Reprinted with permission from K. R. Catchpole, J. Appl. Phys. **102**(1), 013102 (2007). Copyright © 2007 American Institute of Physics.

$$h = \frac{\lambda}{2n_0^{eff}}. \tag{12}$$

When the period of the grating is such that at least two grating modes are excited (for normal incidence, this corresponds to 0th and 3rd grating modes), interference between the grating modes determines the efficiency of excitation of various diffraction modes. Light is efficiently coupled into the 0th diffraction order or the principal diffraction order when the grating height, h is such that the grating modes accumulate a net phase difference of zero. When the net phase shift between the two grating modes is π, most of the light is coupled into the first diffracted order.

For normal incidence, the efficiency of excitation of a grating mode increases as n^{eff} approaches the refractive index of the medium of incidence due to better impedance matching (as discussed earlier in Sec. VII A). This analysis can also be extended to predict the optimum parameters for pillar diffraction gratings.[54]

D. Design of large period gratings

Modal analysis is very effective in predicting the behaviour of rectangular gratings or pillar gratings.[54] Another simple analytical model has been developed to understand and predict/optimize the behaviour of diffraction gratings of arbitrary shape. The technique is applicable only for gratings with periods larger than the wavelength of the incident light, as it is based on scalar diffraction theory.[84,85] In this approach, the transmission function for the periodic arrangement of structures is determined and the corresponding far-field diffraction pattern is computed by applying a Fourier transform.[86] The results of the analytical modelling agree well with the numerical results obtained using FDTD modelling.[87] In this section, we illustrate the approach using gratings depicted in Figure 13, but it can also be used to design periodic structures with arbitrary shapes, as long as the period is larger than the wavelength of incident light.

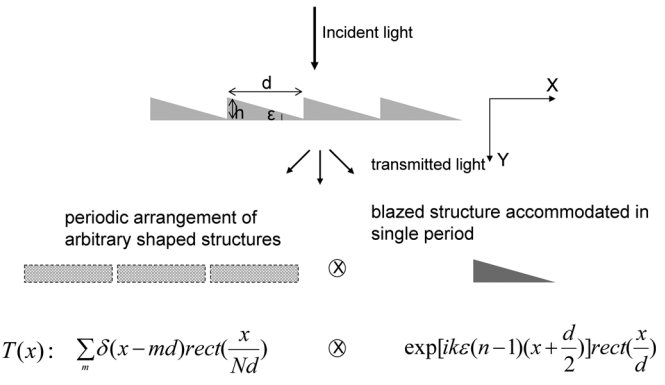

FIG. 13. The grating structure considered for demonstration of the analytical approach. The transmission function of the grating is represented as the convolution of the transmission function of a periodic structure with periodicity d, and a triangular component with base d and height h. N is the number of periods considered for calculations and n is the refractive index of the grating material. The expressions for the transmission functions are indicated below the corresponding structure. Reproduced with permission from S. Mokkapati *et al.*, J. Phys. D: Appl. Phys. **44**(5), 055103 (2011). Copyright © 2011 Institute of Physics.

The structure considered to demonstrate the approach is illustrated in Figure 13. A periodic arrangement of N right-angled prisms with a base dimension of d and height h in air is considered. N has to be a large number for light trapping applications. The total transmission function of the blazed grating $T(x)$ is expressed as the convolution of transmission function of a periodic arrangement (irrespective of the structure within the period) with a period d, $T_{periodic}(x)$, and that of a right angled prism with base d and height h, $T_{prism}(x)$. The periodic transmission function is 1 at integral multiples of d and 0 elsewhere over a spatial range Nd and is expressed as[86]

$$T_{periodic}(x) = \sum_m \delta(x - md) rect\left(\frac{x}{Nd}\right), \tag{13}$$

where $rect(x)$ represents a rectangle function and is defined as $rect(x) = 1$ if $|x| < 1/2$ and 0 elsewhere. Each individual right-angled prism has a transmission of 1 over a width d, but introduces a position (x) dependent phase shift into the transmitted light. Thus, the transmission function of the right-angled prism is expressed as[86]

$$T_{prism}(x) = \exp\left[ik\varepsilon(n-1)\left(x + \frac{d}{2}\right)\right] rect\left(\frac{x}{d}\right), \tag{14}$$

where the exponential term represents the phase function introduced by the prism, k is the wave-vector of the incident light, n is the refractive index of the grating material and the prism angle, and ε is defined as $\tan^{-1}(\frac{h}{d})$.

The far-field light distribution resulting from the grating can now be evaluated using the Fourier transform of the total transmission function.[85] According to the convolution theorem, the Fourier transform of the convolution of two functions is the product of the Fourier transforms of the individual functions. So, the transmitted far-field light distribution due to the grating can now be evaluated from the Fourier transforms of the individual transmission functions represented in Eqs. (13) and (14). Hence the normalized (to the maximum intensity) far-field intensity distribution resulting from transmission through the grating structure becomes[85,86]

$$I(\nu) = I_{periodic}(\nu) I_{prism}(\nu), \tag{15}$$

where $I_{periodic}(\nu)$ is the Fourier transform of $T_{periodic}(x)$ and $I_{prism}(\nu)$ is the Fourier transform of $T_{prism}(x)$. $I_{periodic}(\nu)$ and $I_{prism}(\nu)$ are given by

$$I_{periodic}(\nu) = \sum_m \sin c^2\left[\nu - \frac{m}{d}\right] Nd \tag{16}$$

and

$$I_{prism}(\nu) = \sin c^2\left\{\left[\nu - \varepsilon\frac{n-1}{\lambda}\right] d\right\}, \tag{17}$$

where the *sinc* function is defined as $\sin c(x) = \frac{\sin(\pi x)}{\pi x}$, ν is the position of observation in the Fourier plane, and λ is the wavelength of the incident light.

To gain a conceptual understanding of the effect of varying grating parameters on the intensity distribution of the light transmitted from the grating, we look at the effect of varying the height, *h* of a Si grating on a Si substrate for a fixed period of 1500 nm and an incident wavelength of 800 nm. The far-field intensity distribution from the grating along with the distribution for the periodic arrangement and a single prism are shown in Figure 14 for h = 50, 150, 300, 500, or 600 nm. For h = 50 nm, the intensity distribution of a single prism is concentrated near the 0th order transmission peak of the periodic structure. Hence the net transmission intensity of the grating is mostly concentrated in 0th or principal diffraction order, with only a very small fraction of light coupled into +1 and −1 diffraction orders. When the grating height is increased to 150 nm, the transmission peak from the single prism is centered between the 0th and −1 diffraction orders of the periodic structure, resulting in equal intensity distribution among the 0 and −1 diffraction orders for the grating. Most of the transmitted light is concentrated in these two diffraction orders, with only a small fraction of light coupled into +1 and −2 diffraction orders, as the positions of these diffraction orders coincide with the position of secondary maxima of the prism diffraction pattern. By increasing the grating height to 300 nm, the principal maxima of the prism diffraction pattern coincides exactly with the position of −1 diffraction order of the periodic structure and the position of the rest of diffraction orders of the periodic structure coincide with the minima in the diffraction pattern of the prism. As a result, all the light transmitted from the grating is coupled into −1 diffraction order. By increasing the grating height to 500 nm, the principal maxima in the prism diffraction pattern moves closer to −2 diffraction order of the periodic structure. In this case, the light transmitted from the grating is mostly coupled to −1 and −2 diffraction orders, with a larger fraction being coupled into the −2 diffraction order.

For light trapping applications, a large fraction of the light transmitted from the grating should be coupled into diffraction orders propagating outside the escape cone of Si. For incident light with wavelength of 800 nm (at 800 nm, refractive index of Si is 3.67), the half-angle for the escape cone calculated using Snell's law is 15.8°. For a period of 1500 nm (the parameter chosen in Figure 14), ±1 diffraction orders propagate at an angle of 8.4° and ±2 diffraction orders propagate at an angle of 16.9° with respect to the surface normal. So, light should be coupled into ±2 or higher diffraction orders for trapping inside Si. For a grating height of 500 nm, a large fraction of the transmitted light is trapped inside Si. For all the transmitted light to be trapped, a grating height of at least 600 nm should be chosen, as for this condition the principal maxima in the diffraction pattern of the prism coincides with the position of −2 diffraction order of the periodic structure. All the transmitted light of wavelength 800 nm will be trapped for grating heights larger than 600 nm.

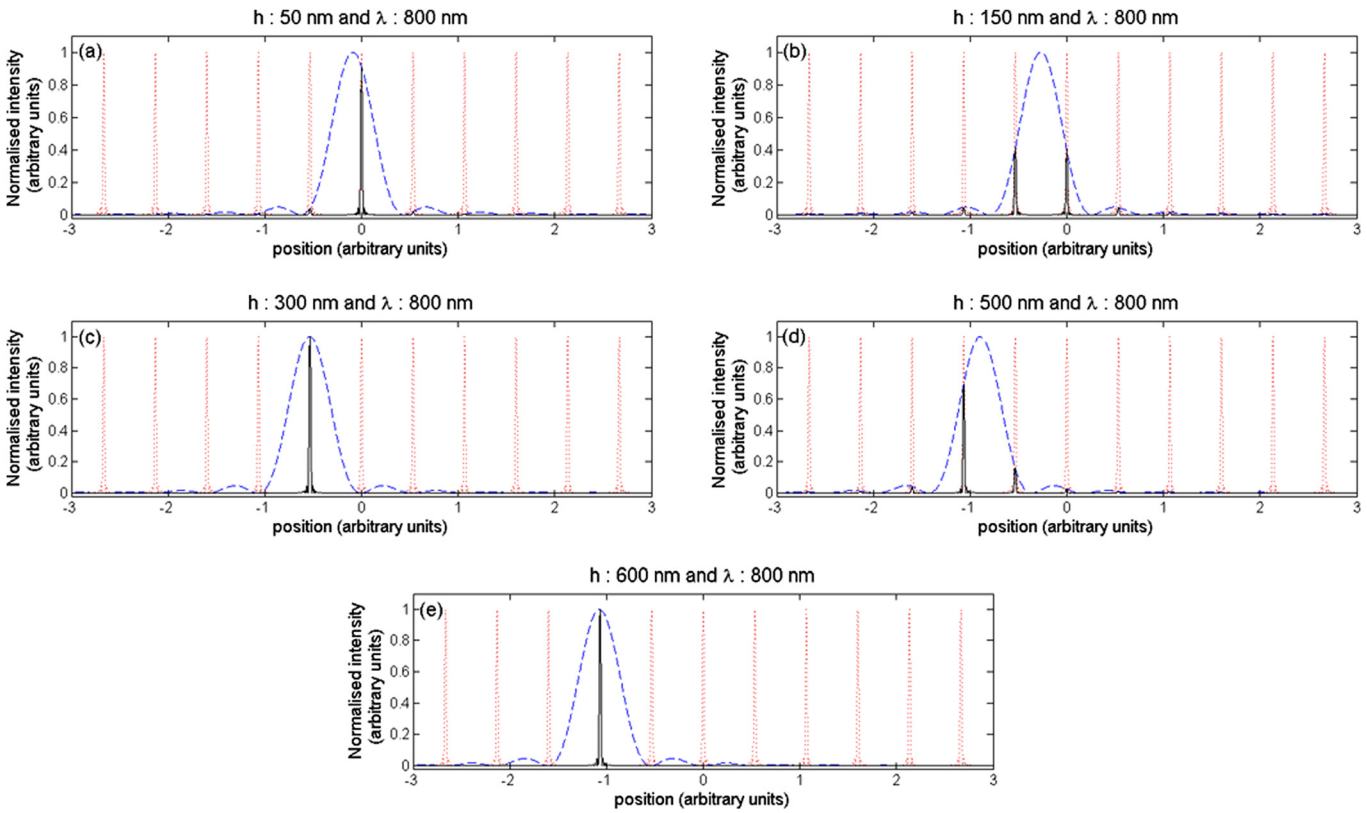

FIG. 14. Normalized transmitted intensity distribution of a Si grating with a period, d 1500 nm. The intensity distribution of the periodic arrangement (obtained using Eq. (16)) is represented in red, while the intensity distribution from a single prism (obtained using Eq. (17)) is represented in blue and the net intensity (evaluated using Eq. (15)) is represented in black. The wavelength of the incident light is fixed at 800 nm and the grating height is (a) 50 nm, (b) 150 nm, (c) 300 nm, (d) 500 nm, or (e) 600 nm. Reproduced with permission from S. Mokkapati *et al.*, J. Phys. D: Appl. Phys. **44**(5), 055103 (2011). Copyright © 2011 Institute of Physics.

E. Fundamental limits with gratings

The above approaches are simple means of optimizing a large period ($d > \lambda$) grating performance. However, the fundamental question of whether or not diffraction gratings can match or exceed the path length enhancement of $4n^2$ obtained using an ideal Lambertian surface on a weakly absorbing bulk substrate still needs to be addressed. The ray-optics approach used for analysing the light trapping in a bulk substrate using a Lambertian surface cannot be used to analyse the case of dielectric gratings with wavelength scale periodicity or when only a few modes are allowed in the substrate (i.e., for thin substrates with thickness comparable to the wavelength of incident light). Yu *et al.*[80] studied the case of periodic gratings on semiconductors using a statistical temporal coupled mode theory.[88]

Periodic diffraction gratings couple incident plane waves to guided optical modes inside a thin semiconductor absorber whose in-plane wavevector satisfies Eq. (8). Each of these guided optical modes can in turn couple to plane waves in air whose wavevectors also satisfy Eq. (8). As discussed earlier, for propagating plane waves, the in-plane wavevectors lie within a circle of radius $n\frac{2\pi}{\lambda}$ in k-space, where n is the refractive index of the medium (air or the absorbing layer). In the limit where the absorption in the active volume is weak, the maximum path length enhancement, F that can be achieved by coupling incident light into guided optical modes inside the absorber through a diffraction grating is given by[80]

$$F = \frac{2\pi c}{t\Delta\omega}\frac{M}{N}, \tag{18}$$

where t is the thickness of the absorber, $\Delta\omega$ is the bandwidth of the incident radiation, M is the number of guided optical modes supported by the absorber, and N is the number of free space propagating modes.

For a single period diffraction grating schematically represented in Figure 15(a), the allowed diffraction modes in air are separated from each other by $\frac{2\pi}{d}$ in k-space. Moreover, the wavevector of the propagating modes should lie within a circle of radius $|k_0|$, the wavevector of incident light (Figure 15(b)). For large period gratings, i.e., $d \gg \lambda$, the number of free space propagating modes at a wavelength λ is given by

$$N = \frac{2d}{\lambda}. \tag{19}$$

In the frequency range $(\omega, \omega + \Delta\omega)$, the number of guided modes supported by the absorbing layer is (Figure 15(c))

$$M = \frac{2n^2\pi\omega}{c^2}\frac{d}{2\pi}\frac{t}{2\pi}\Delta\omega. \tag{20}$$

Combining Eqs. (18)–(20), for single period gratings with periodicity much larger than the wavelength of incident light, the maximum path length enhancement achievable is πn. This upper bound on the path length enhancement is lower than the Lambertian limit of $4n^2$, but equal to the 2D enhancement limit for the case of geometrical optics.

From Eq. (18), we see that the upper bound on the path length enhancement can be maximised by minimising the number of free space propagating diffraction modes, N and maximising the guided optical modes in the absorber, M. The number of free space propagating diffraction modes is minimised by choosing a grating period smaller than or equal to the wavelength of incident light ($d \leq \lambda$). Only one free space propagating mode, the 0th or principal diffraction order exists for such gratings. However, the number of guided optical modes, M increases linearly with the frequency of incident light (Eq. (20)) or decreases inversely with the wavelength of incident light. So, the upper bound on the maximum path length enhancement for a single period grating is maximised for $d = \lambda$ and reaches a value of $2\pi n$.[80]

The maximum achievable absorption enhancement can be increased further by increasing the number of guided optical modes in the absorber, M by using bi-periodic gratings with periodicity equal to the wavelength of incident light. The minimum number of free space propagating modes for a bi-period grating are $N = 2$, one for each polarisation. The

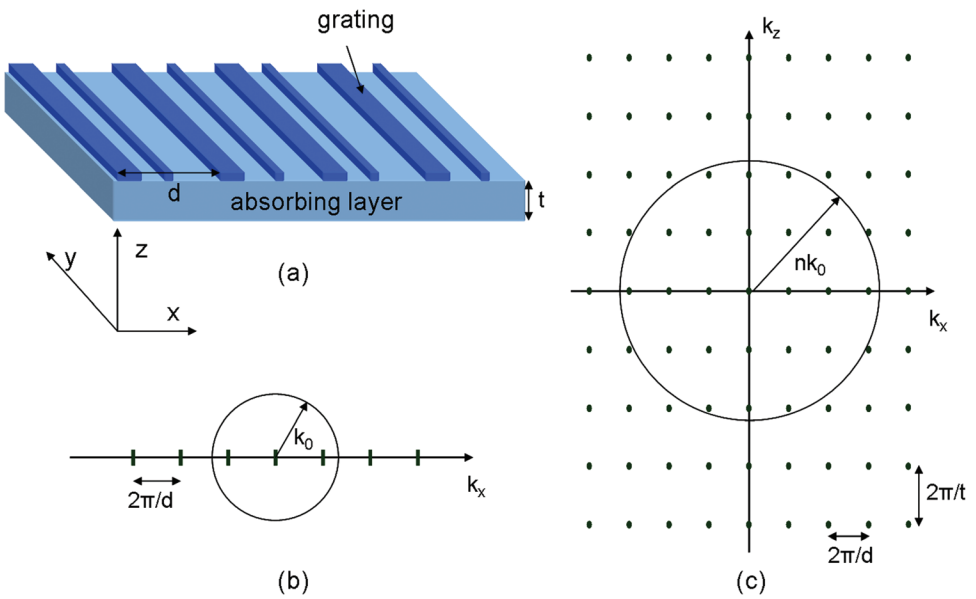

FIG. 15. (a) Schematic of a single-period grating with periodicity d in x-direction. (b) Diffraction modes (in air) in k-space. (c) Diffraction modes in the absorbing medium with thickness t.

total number of guided optical modes supported by the absorber in the frequency range $(\omega, \omega + \Delta\omega)$ is

$$M = \frac{8n^3\pi\omega^2}{c^3}\left(\frac{d}{2\pi}\right)^2 \frac{t}{2\pi}\Delta\omega. \quad (21)$$

Using Eqs. (18) and (21), the upper bound on the maximum path length enhancement achievable with bi-periodic gratings is $4\pi n^2$.[80] As the period of the grating increases, the number of free space propagating modes increases and for a bi-periodic grating with period much larger than the incident wavelength ($d > \lambda$), the upper bound on absorption enhancement approaches that of the Lambertian case ($4n^2$).[80]

Bermel *et al.*[27] have experimentally demonstrated that bi-periodic gratings result in better performance than single-period gratings. Numerical studies by Mallick *et al.*[89] show that the Lambertian limit for light trapping can be exceeded for normal incidence using bi-periodic gratings. Tobias *et al.*[90] also showed that bi-periodic gratings are better than single-period gratings and can exceed the Lambertian limit for path length enhancement in a narrow band using the theory of periodic radiation arrays.

F. Angular dependence and light trapping

Using geometrical optics, it can be shown that the path length enhancement increases from $4n^2$ to $4n^2/\sin^2\theta$ for a restricted acceptance half-angle of θ.[91] The acceptance angle also restricts the maximum useful concentration for a cell, since a cell with maximum concentration (46 000 suns) must accept light from all angles. Thus, the maximum useful concentration ratio for a cell of acceptance half-angle θ is $46\,000 \sin^2\theta$, e.g., 350 for a cell of acceptance half angle 5°.

The relation $4n^2/\sin^2\theta$ comes fundamentally from the conservation of étendue and radiance, valid for layers that are sufficiently thick that they support many optical modes. Radiance is given by $R = B/n^2$, where B is the brightness (intensity per unit solid angle, W/cm^2/steradian). It is conserved in a bundle of rays in a lossless medium.[92,93] Tobias *et al.* have shown that étendue is also conserved when light is diffracted by a grating into a thick substrate,[94] i.e., for grating structures as well as for structures that can be described with geometrical optics, there is a trade-off between maximum enhancement and angular response. Since many structures such as random surfaces can be accurately modeled as large period gratings, this is a quite general limit. In addition, Yu and Fan[95] have calculated the upper limit for the integrated (over varying angles of incidence) absorption enhancement factors that can be achieved by using dielectric gratings using the analysis developed in Ref. 96. Their analysis also shows that the angle-integrated upper limit for the absorption enhancement is lower for small period gratings compared to large period structures.

The sensitivity of the grating response to the angle of incidence of light is schematically illustrated in Figures 16(a) and 16(b). The solid dots in the figures show the diffraction modes in k-space for normal incidence. The position of the diffraction modes for off-normal incidence is shifted with respect to that for normal incidence and is represented by open dots. The solid and open dots within the red circle represent the propagating diffraction orders for normal and off-normal incidence, respectively. The relative change in the number of propagating diffraction modes for off-normal incidence is smaller for the large period grating (Figure 16(a)) than for the small period grating (Figure 16(b)). The relatively small change in the number of propagating diffraction modes for large period gratings makes them less sensitive to the angle of incidence than small period gratings. For small period gratings, the number of propagating diffraction modes is considerably reduced for off-normal incidence. So, small period gratings can effectively couple only to normally incident light. Relatively larger periods would be expected to provide better coupling over a range of incident angles over the day, since small periods can only couple effectively to normally incident light.

The trade-off between enhancement and angular response has also been highlighted by Sheng *et al.*, who showed that the enhancement for a 2D (single period) structure can be as high as $2.7\pi n$ for normally incident light, considerably larger than the Lambertian value of πn for 2D scattering.[97] However, they found that the πn limit still applied to their structure for isotropically incident light.

G. Asymmetric gratings

Having determined the limit of light trapping with grating structures, the question arises as to what types of

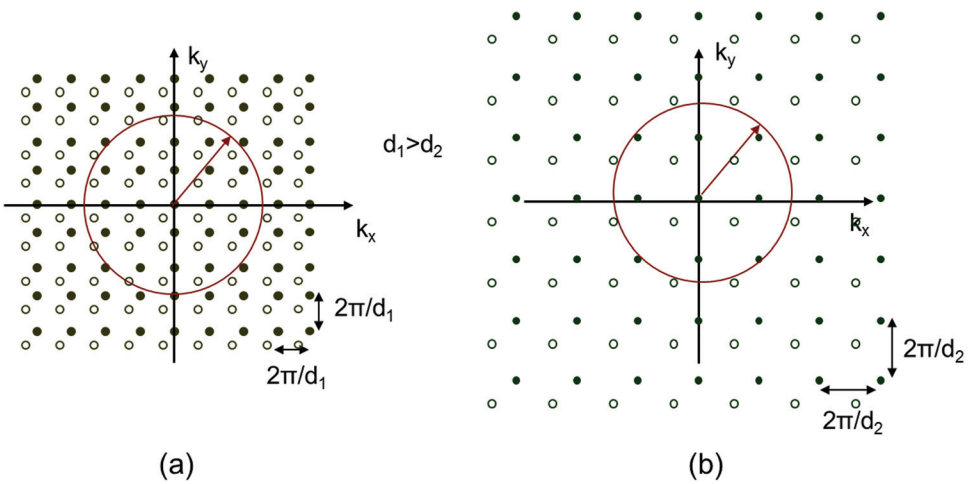

FIG. 16. (a) and (b) Schematic demonstration of the effect of grating period on the angular dependence of its response. The solid green dots represent the allowed diffraction modes in k-space (reciprocal space) for normal incidence. The hollow green dots represent the shift in the position of the modes for off-normal incidence. The areas bounded by the circles represent the allowed in-plane k vectors for the propagating modes supported by the medium. The radii of the circles are |k|.

structures can approach that limit. An important parameter to consider here is the symmetry of the grating. A symmetric grating can efficiently couple out the light from the active volume of the cell to an outgoing mode just as it couples incoming light into the active volume (Figure 17(a)). According to the reciprocity theorem, the coupling efficiency of the diffracted light to the outgoing wave is same as the coupling efficiency of the incident wave to the diffraction modes. It has been proposed that the out-coupling of light from the solar cell active volume can be reduced by introducing asymmetry into the grating structure,[98,99] as illustrated in Figure 17(b).

The theoretical approaches presented in Sec. VII F can be used to determine whether asymmetry in gratings is beneficial for light trapping. From the simple analytical model based on scalar diffraction theory presented earlier, it can be seen that the diffraction orders into which most light is coupled are determined by the phase shift introduced by the grating element. This phase shift is the same for light incident from air side on to the grating or from the active volume on to the grating. For achieving light trapping and reducing the out-coupling of light from the active volume to air, the following two conditions have to be satisfied: (a) The phase shift introduced by the grating element should be such that light is coupled into higher order diffraction modes inside the cell and (b) Higher order diffraction modes do not exist in air. For small period gratings, higher order diffraction modes do not exist in air and introducing asymmetry into the grating structure directs incident light into higher order diffraction modes inside the cell for small aspect ratios, compared to symmetric structures. For large period gratings ($d > \lambda$), higher order diffraction modes exist in air and introducing asymmetry into the grating structure does not reduce out-coupling of light.

These results are consistent with the extensive analysis presented by Yu *et al.* for estimating the upper bound of absorption enhancement using gratings.[80] The upper bounds on the maximum path length enhancement achievable by diffraction gratings discussed in Sec. VII E were derived assuming that the incident plane waves can couple to all guided modes inside the absorber and all free space propagating diffraction modes. This is only true for asymmetric gratings. For a symmetric grating, the guided optical modes in the absorber either have an odd or even modal profile. Normally incident plane wave has an even modal profile and cannot couple to guided optical modes with odd profiles. For single period, wavelength scale gratings, the number of free space propagating modes is still 1, but the number of accessible guided modes is halved due to symmetry constraints, reducing the upper bound on the maximum path length enhancement achievable to πn. However, for large single-period ($d > \lambda$) gratings, the number of accessible free space propagating modes is also halved, as the incident plane wave can only couple to free space propagating modes with symmetric modal profile. So, the upper bound on the absorption enhancement is not altered by symmetry considerations.

From the above analysis, wavelength scale asymmetric bi-periodic gratings should result in the best light trapping for grating structures. Han and Chen[100] have demonstrated using group theory that the Lambertian light trapping limit can be exceeded using asymmetric sub-wavelength scale bi-periodic gratings. Chong *et al.* have shown numerically that the overall J_{sc} for a skewed pyramid structure on the rear of a solar cell can reach the Lambertian value, and that the enhancement exceeds Lambertian for particular wavelength ranges.[68]

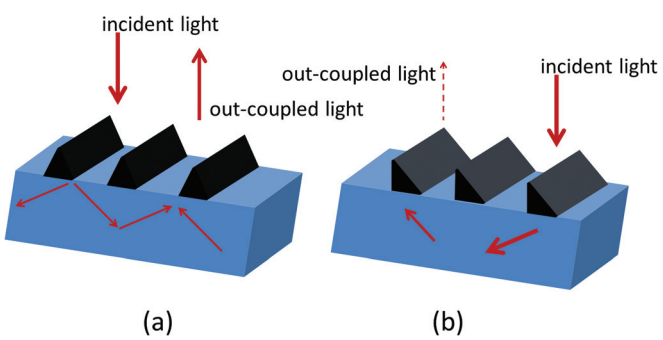

FIG. 17. Schematic illustration of (a) out-coupling of light from a solar cell with a symmetric grating structure and (b) reduced out-coupling by introducing asymmetry into the grating structure.

VIII. OTHER LIGHT TRAPPING STRUCTURES

There are a variety of other structures that can be used for nanophotonic light trapping in solar cells. The most common methods are plasmonic structures, random scattering surfaces, and nanowires. These are only discussed briefly here. In the case of plasmonics, this is because there have already been several good reviews published recently. For random scattering surfaces, very good experimental enhancements have been achieved, but the strongly photonic and irregular nature of the surface means that it is more difficult to gain physical insight into their behaviour. There is likely to be much more work done in this area in the coming years. Nanowires are a younger subject, where very impressive optical enhancements have been achieved. The major challenge in this field is likely to be electrical rather than optical.

A. Plasmonic structures

A plasmon is a collective oscillation of electrons in a metal. Plasmonic light trapping involves either localized surface plasmons supported by discrete metal nanoparticles or surface plasmon polaritons supported by continuous metal films. Discrete metal nanoparticles can be used as efficient scatterers to couple incident sunlight into trapped modes in thin solar cells. This was first demonstrated by Stuart and Hall[101] and subsequently by several other researchers.[102–107] Random arrays of metal nanoparticles deposited on a solar cell surface behave as a random scattering surface with tunable scattering resonance. Periodic arrays of metal nanoparticles have also been studied for light trapping applications and optimized using grating theory.[70] The concentrated near field of metal nanoparticles embedded within a strongly absorbing semiconductor can be used to enhance absorption in nearby semiconductor and result in enhanced photocurrent generation from a thin solar cell.[108–113] Structured,

continuous metal surfaces can be used to couple incident light either to plasmonic interface modes or photonic waveguide modes propagating inside the semiconductor. For weak absorbers like c–Si, it is advantageous to couple to waveguided modes to avoid losses in the plasmonic modes.[114] A detailed overview of plasmonic light trapping can be found in Refs. 115–118.

B. Random scattering surfaces

Random scattering surfaces are easy to fabricate and effectively trap light over a wide angular and wavelength range with minimal parasitic absorption.[119,120] The a-Si:H solar cells and tandem solar cells fabricated by Kaneka use random texturing of transparent conducting oxide (TCO) front contact on glass superstrates for achieving light trapping.[121,122] The highest reported efficiency for an a-Si:H solar cell and a nanocrystalline Si solar cell is 10.1 ± 0.3 and 10.1 ± 0.2, respectively.[123] The highest reported efficiency for a tandem a-Si/microcrystalline Si thin film solar cell and submodule is 11.9 ± 0.8 and 11.7 ± 0.4, respectively.[123]

Because of the complexity of the interaction of these surfaces with light, there is limited theoretical guidance for the design of these surfaces. However, it has been shown that it will be advantageous to direct light outside the escape cone[124] and that criteria for the depth of local features can be derived.[125] Random scattering surfaces can be theoretically studied using grating theories by treating them as periodic structures with very large period.

As with grating structures, increased surface area can lead to increased surface recombination and steep features can lead to reduced material quality if deposited on a textured surface. If the design includes a conformal metal reflector, it will be also important to minimise coupling to the metal because structured metals can be very strongly absorbing.[126,127]

C. Nanowires

Solar cells based on nanowires have been investigated recently. Nanowire solar cells are fabricated from arrays of long semiconductor cylinders, usually arranged vertically but not necesssarily periodically. An example structure is shown in Figure 6(d). Nanowire structures are strongly photonic, and it has been shown that nanowires can lead to excellent light trapping.[128–130] It has been demonstrated by Kelzenberg *et al.* that nanowire arrays with a packing fraction around 5% can achieve similar to Lambertian ($4n^2$) absorption for an equivalent thickness silicon layer.[128] This very high absorptance for such a low packing fraction suggests that their properties may be more due to the individual nanowires than to a collective, grating-like effect, and indeed, simulations have shown that waveguiding within the nanowire is the most important effect. Sturmberg *et al.* have shown that the enhanced absorption in nanowire arrays can be attributed to a few modes of the array, which couple well to incident light, overlap well with the nanowires, and exhibit strong Fabry-Pérot resonances.[131] Path length enhancements of up to 73 have been demonstrated for normal incidence for silicon nanowire arrays on silicon substrates.[129]

The p-n junction in these solar cells is often formed radially in these devices, which has the advantage of separating the functions of charge carrier collection and optical absorption.[132] The growth of very good material quality[133] and other advantages have also been demonstrated, including the ability to detach the nanowire structure from the growth substrate.[134] Device modelling has shown that efficiencies of 20% may be possible with CdS/CdTe nanowire solar cells,[135] and promising experimental cell efficiencies have been reported for silicon,[136,137] III-nitrides,[138] and for Si/GaN heterojunctions.[139] The main challenge associated with the radial design is the need for very low recombination in the junction region,[132,140,141] which may lead to this design being most suitable for certain material systems.[135]

D. Fundamental limits with general nanophotonic structures

In the above sections, we first described the fundamental limit for bulk semiconductors with isotropically scattering, geometrical scale features (the Lambertian case of $4n^2$ enhancement).[10] A Lambertian surface or an isotropic surface ensures that the probability of coupling light into all available optical modes is the same. The optical mode density in air or in the absorbing layer is not altered. Scattering structures such as nanoparticles on the surface of a relatively thick solar cell are likely to mimic an isotropic or a perfectly randomizing surface in most cases. Assuming there is no change in the density of optical modes supported in air or by the absorbing layer brought about by the nanoparticles, the Lambertian limit for light trapping cannot be exceeded by scatterers on relatively thick substrates. If we eliminate the parasitic losses in the scatterers, the best we can do is approach the $4n^2$ limit.

If the mode density in the absorbing layer is reduced, the maximum path length enhancement achievable falls below the $4n^2$ limit, assuming that the efficiency of coupling light into all available optical modes remains the same. This is the case for thin active layers and a random light trapping structure. For very thin active layers, the optical mode density is not continuous. The active layer now acts as a waveguiding layer and only supports a discrete set of optical modes. A reduced mode density in the active layer means reduced intensity and hence the maximum path length enhancement that can be achieved in this case is smaller than $4n^2$.[142]

Again, assuming that the efficiency of coupling light into all available optical modes remains the same, the path length enhancement for the Lambertian case can be exceeded by either reducing the number of optical modes in air or by increasing the number of optical modes outside the escape cone in the absorbing layer or both.

With a diffraction grating, the periodicity of the grating along with the index of the absorbing layer determines the number of optical modes allowed in air and in the absorbing medium. The maximum absorption enhancement is obtained by maximizing the number of modes (outside escape cone)

TABLE I. Summary of maximum limit for light trapping and analysis techniques for different structures.

Structure	Analysis	Maximum limit for light trapping	References
	Grating period, d « wavelength, λ		
Single period	Photonic crystal equation or effective medium theory	No light trapping, anti-reflection only	36, 49, 56, and 57
Bi-periodic	Effective medium theory		
	Grating period, $d \sim$ wavelength, λ		
Single period	Statistical temporal coupled mode theory	$2\pi n$ for asymmetric πn for symmetric (*n: refractive index of a high index substrate*)	68
Bi-periodic	Statistical temporal coupled mode theory	$4\pi n^2$ for asymmetric $2\pi n^2$ for symmetric	68
	Grating period, d » wavelength, λ or random structures (as $d \rightarrow \infty$)		
Single period	Statistical temporal coupled mode theory	πn	68
Random, 2D (grating in the limit $d \rightarrow \infty$)	Geometrical optics		Following method of Ref. 4
Bi-periodic	Statistical temporal coupled mode theory	$4n^2$	38
Random (grating in the limit $d \rightarrow \infty$)	Geometrical optics		10
	Other structures		
Waveguide on mirror	Density of modes	$4n^2 + n\lambda/h$	135
Ultrathin low index waveguide in high index cladding	Thin film optics	$4n_2^2\left[\frac{2}{3}\frac{n_1}{n_2}+\frac{1}{3}\left(\frac{n_1}{n_2}\right)^5\right]$	134
Structures with enhanced LDOS	Statistical temporal coupled mode theory, LDOS analysis	$>4n^2$	84, 132, and 133

in the absorber and simultaneously minimizing the number of modes in the air. This leads to a maximum enhancement of $4\pi n^2$ for a wavelength scale, bi-periodic grating.[80] Since there is only one optical mode supported in air (the principal diffraction order), the structure becomes very sensitive to the angle of incidence. It was also shown that étendue is conserved for grating structures, as it is for those that can be described by geometric optics.[94] Hence, for both types of structures, there is a trade-off between enhancement at normal incidence and the angular response.

Alternatively, absorber layers can be designed that support enhanced density of optical modes, without altering the mode density in air, in order to go beyond the $4n^2$ limit. Callahan *et al*. have shown that light trapping beyond the $4n^2$ limit can be achieved provided that the structure has an increased local density of optical states (LDOS) compared to the bulk semiconductor.[143] The dispersion relations of the waveguide structure can be used to predict the absorption enhancement achievable.[144] An example of a structure with an absorption beyond $4n^2$ is a thin waveguide surrounded by a higher refractive index medium.[145] This structure makes use of tunneling evanescent waves to increase the absorption. Schiff has also shown that for a relatively thick waveguide on a metal, the fundamental limit to light trapping is given by $4n^2 + n\lambda/h$, with the extra enhancement due to a plasmonic mode at the metal semiconductor interface.[146] However, absorption in the metal is a signficant issue. More generally, Yu *et al*. have shown that the $4n^2$ limit can be surpassed if the structure exhibits deep subwavelength confinement of optical modes.[96] For all of these structures with very high potential enhancements, it will be important to include the consideration of parasitic losses, as discussed in Sec. IV. The various fundamental limits for different structures are summarized in Table I.

IX. SUMMARY

Nanophotonics is essential for increasing the absorption in thin film solar cells. To develop effective designs, it is important first to gain an understanding of the potential of light trapping to provide absorption enhancement, in strongly or weakly absorbing materials, including the effects of optical and electrical losses. Periodic photonic structures are important in their own right and also provide the best developed starting point for insight into the physical mechanisms involved in nanophotonic light trapping. Other structures are also very promising for light trapping, and some of the ideas developed for periodic structures are also transferrable to these contexts. This field is developing very rapidly, and there may also be interesting synergies with other areas of photovoltaics that have not yet been imagined.

ACKNOWLEDGMENTS

One of the authors (KRC) would like to dedicate this paper to Rudolf Morf, who first sparked her interest in diffractive structures for solar cells. This work has been supported by the Australian Research Council and the Australian Solar Institute.

[1]International Energy Agency (02.05.2011). *World energy outlook 2010 Executive summary*. Available at: http://www.worldenergyoutlook.org/docs/weo2010/WEO2010_ES_English.pdf.

[2]Solarbuzz. *Solar Market Research and Analysis*. Available at: http://www.solarbuzz.com/going-solar/understanding/technologies.
[3]M. A. Green, K. Emery, Y. Hishikawa, and W. Warta, Prog. Photovoltaics **18**(5), 346 (2010).
[4]P. Campbell and M. A. Green, J. Appl. Phys. **62**(1), 243 (1987).
[5]P. Campbell, S. R. Wenham, and M. A. Green, Sol. Energy Mater. Sol. Cells **31**(2), 133 (1993).
[6]P. Campbell, Sol. Energy Mater. **21**(2–3), 165 (1990).
[7]P. Campbell, J. Opt. Soc. Am. B **10**(12), 2410 (1993).
[8]P. Campbell and M. A. Green, J. Appl. Phys. **62**(1), 243 (1987).
[9]K. J. Weber and A. W. Blakers, Prog. Photovoltaics **13**(8), 691 (2005).
[10]E. Yablonovitch and G. D. Cody, IEEE Trans. Electron Devices **29**(2), 300 (1982).
[11]A. Göetzberger, in 15th Photovoltaic Specialists Conference, Kissimmee, FL, 1981.
[12]E. Yablonovitch, J. Opt. Soc. Am. **72**(7), 899 (1982).
[13]R. Brendel, in *Thin-Film Crystalline Silicon Solar Cells* (Wiley-VCH, 2005).
[14]M. A. Green, Prog. Photovoltaics **10**, 235 (2002).
[15]M. A. Green, Prog. Photovoltaics **7**(4), 327 (1999).
[16]O. D. Miller and E. Yablonovitch, arxiv preprint arXiv:1106.1603, 2011.
[17]G. Smestad and H. Ries, Sol. Eng. Mater. Sol. Cells **25**, 51 (1992).
[18]R. T. Ross, J. Phys. Chem. **46**, 4590 (1967).
[19]A. Polman and H. A. Atwater, Nature Mater. **11**(3), 174 (2012).
[20]T. Trupke, J. Zhao, A. Wang, and M. A. Green, paper presented at the Conference on Optoelectronic and Microelectronic Materials and Devices, Sydney, 2002.
[21]M. Werner, U. Schubert, C. Hagendorf, J. Schneider, M. Keevers, and R. Egan, in *Proceedings of the 24th European Photovoltaic Solar Energy Conference* (Hamburg, 2009), p. 2482.
[22]X. Li, N. P. Hylton, V. Giannini, K.-H. Lee, N. J. Ekins-Daukes, and S. A. Maier, "Multi-dimensional modeling of solar cells with electromagnetic and carrier transport calculations," Prog. Photovolt: Res. Appl. (to be published).
[23]X. Li, N. P. Hylton, V. Giannini, K.-H. Lee, N. J. Ekins-Daukes, and S. A. Maier, Opt. Express **19**(S4), A888 (2011).
[24]P. Basore, in *IEEE Photovoltaic Specialists Conference* (1993), p. 147.
[25]Y. Yang, S. Pillai, H. Mehrvarz, H. Kampwerth, A. Ho-Baillie, and M. A. Green, "Enhanced light trapping for high efficiency crystalline solar cells by the application of rear surface plasmons," Sol. Eng. Mater. Sol. Cells **101**, 217–226 (2012).
[26]T. Trupke, E. Daub, and P. Wuerfel, Sol. Eng. Mater. Sol. Cells **53**, 103 (1998).
[27]P. Bermel, C. Luo, L. Zeng, L. C. Kimerling, and J. D. Joannopoulos, Opt. Express **15**(25), 16986 (2007).
[28]A. Chutinan, N. P. Kherani, and S. Zukotynski, Opt. Express **17**(11), 8871 (2009).
[29]O. El Daif, E. Drouard, G. Gomard, A. Kaminski, A. Fave, M. Lemiti, S. Ahn, S. Kim, P. Roca i Cabarrocas, H. Jeon, and C. Seassal, Opt. Express **18**(S3), A293.
[30]Erik Garnett and Peidong Yang, Nano Letters **10** (3), 1082 (2010).
[31]M. D. Kelzenberg, S. W. Boettcher, J. A. Petykiewicz, D. B. Turner-Evans, M. C. Putnam, E. L. Warren, J. M. Spurgeon, R. M. Briggs, N. S. Lewis, and H. A. Atwater, Nature Mater. **9**(3), 239 (2010).
[32]Z. Fan, H. Razavi, J.-W. Do, A. Moriwaki, O. Ergen, Y.-L. Chueh, P. W. Leu, J. C. Ho, T. Takahashi, L. A. Reichertz, S. Neale, K. Yu, M. Wu, J. W. Ager, and A. Javey, Nature Mater. **8**(8), 648 (2009).
[33]K. R. Catchpole, S. Mokkapati, F. Beck, E.-C. Wang, A. McKinley, A. Basch, and J. Lee, MRS Bull. **36**, 461 (2011).
[34]R. Dewan, M. Marinkovic, R. Noriega, S. Phadke, A. Salleo, and D. Knipp, Opt. Express **17**(25), 23058 (2009).
[35]H. Sai, Y. Kanamori, K. Arafune, Y. Ohshita, and M. Yamaguchi, Prog. Photovoltaics **15**(5), 415 (2007).
[36]Y. Kanamori, M. Sasaki, and K. Hane, Opt. Lett. **24**(20), 1422 (1999).
[37]T. K. Gaylord, W. E. Baird, and M. G. Moharam, Appl. Opt. **25**(24), 4562 (1986).
[38]S. Chih-Hung, M. Wei-Lun, C. L. Nicholas, J. Peng, and J. Bin, Appl. Phys. Lett. **91**(23), 231105 (2007).
[39]S. Chih-Hung, J. Peng, and J. Bin, Appl. Phys. Lett. **92**(6), 061112 (2008).
[40]C. Eisele, C. E. Nebel, and M. Stutzmann, J. Appl. Phys. **89**(12), 7722 (2001).
[41]L. Francisco and T. Ignacio, J. Appl. Phys. **100**(12), 124504 (2006).
[42]Y. M. Song, J. S. Yu, and Y. T. Lee, Opt. Lett. **35**(3), 276 (2010).
[43]A. Gombert, W. Glaubitt, K. Rose, J. Dreibholz, B. Bläsi, A. Heinzel, D. Sporn, W. Döll, and V. Wittwer, Thin Solid Films **351**(1–2), 73 (1999).
[44]A. Gombert, W. Glaubitt, K. Rose, J. Dreibholz, B. Bläsi, A. Heinzel, D. Sporn, W. Döll, and V. Wittwer, Sol. Energy **68**(4), 357 (2000).
[45]K. Forberich, G. Dennler, M. C. Scharber, K. Hingerl, T. Fromherz, and C. J. Brabec, Thin Solid Films **516**(20), 7167 (2008).
[46]M. Auslender, D. Levy, and S. Hava, Appl. Opt. **37**(2), 369 (1998).
[47]L. Escoubas, J.-J. Simon, P. Torchio, D. Duché, S. Vedraine, W. Vervisch, J. Le Rouzo, F. Flory, G. Rivière, G. Yeabiyo, and H. Derbal, Appl. Opt. **50**(9), C329 (2011).
[48]J. Zhu, Z. Yu, G. F. Burkhard, C.-M. Hsu, S. T. Connor, Y. Xu, Q. Wang, M. McGehee, S. Fan, and Y. Cui, Nano Lett. **9**(1), 279 (2008).
[49]A. Gombert, K. Rose, A. Heinzel, W. Horbelt, C. Zanke, B. Bläsi, and V. Wittwer, Sol. Energy Mater. Sol. Cells **54**(1–4), 333 (1998).
[50]R. Bräuer and O. Bryngdahl, Appl. Opt. **33**(34), 7875 (1994).
[51]S. Mishra and S. Satpathy, Phys. Rev. B **68**(4), 045121 (2003).
[52]P. Sheng, R. S. Stepleman, and P. N. Sanda, Phys. Rev. B **26**(6), 2907 (1982).
[53]G. Lifante, Phys. Scr. **2005**(T118), 72.
[54]K. R. Catchpole and M. A. Green, J. Appl. Phys. **101**(6), 063105 (2007).
[55]D. H. Raguin and G. Michael Morris, Appl. Opt. **32**(14), 2582 (1993).
[56]Y. Ono, Y. Kimura, Y. Ohta, and N. Nishida, Appl. Opt. **26**(6), 1142 (1987).
[57]E. N. Glytsis and T. K. Gaylord, Appl. Opt. **31**(22), 4459 (1992).
[58]E. B. Grann, M. G. Varga, and D. A. Pommet, J. Opt. Soc. Am. A **12**(2), 333 (1995).
[59]S. A. Boden and D. M. Bagnall, Prog. Photovoltaics **18**(3), 195 (2010).
[60]Y. Kanamori, K. Hane, H. Sai, and H. Yugami, Appl. Phys. Lett. **78**(2), 142 (2001).
[61]P. Sheng, A. N. Bloch, and R. S. Stepleman, Appl. Phys. Lett. **43**(6), 579 (1983).
[62]L. Zeng, Y. Yi, C. Hong, J. Liu, N. Feng, X. Duan, L. C. Kimerling, and B. A. Alamariu, Appl. Phys. Lett. **89**(11), 111111 (2006).
[63]D. Zhou and R. Biswas, J. Appl. Phys. **103**(9), 093102 (2008).
[64]J. G. Mutitu, S. Shi, C. Chen, T. Creazzo, A. Barnett, C. Honsberg, and D. W. Prather, Opt. Express **16**(19), 15238 (2008).
[65]F. Ning-Ning, J. Michel, Z. Lirong, L. Jifeng, H. Ching-Yin, L. C. Kimerling, and D. Xiaoman, IEEE Trans. Electron Devices **54**(8), 1926 (2007).
[66]L. Zeng, P. Bermel, Y. Yi, B. A. Alamariu, K. A. Broderick, J. Liu, C. Hong, X. Duan, J. Joannopoulos, and L. C. Kimerling, Appl. Phys. Lett. **93**(22), 221105 (2008).
[67]L. Zhao, Y. H. Zuo, C. L. Zhou, H. L. Li, H. W. Diao, and W. J. Wang, Sol. Energy **84**(1), 110 (2010).
[68]T. Kong Chong, J. Wilson, S. Mokkapati, and K. R. Catchpole, J. Opt. A, Pure Appl. Opt. **14**, 024012 (2012).
[69]K. Xingze Wang, Z. Yu, V. Liu, Y. Cui, and S. Fan, Nano Lett. **12**(3), 1616 (2012).
[70]S. Mokkapati, F. J. Beck, A. Polman, and K. R. Catchpole, Appl. Phys. Lett. **95**(5), 053115 (2009).
[71]H. Sai, H. Fujiwara, M. Kondo, and Y. Kanamori, Appl. Phys. Lett. **93**(14), 143501 (2008).
[72]U. W. Paetzold, E. Moulin, D. Michaelis, W. Bottler, C. Wachter, V. Hagemann, M. Meier, R. Carius, and U. Rau, Appl. Phys. Lett. **99**(18), 181105 (2011).
[73]V. E. Ferry, M. A. Verschuuren, M. Claire van Lare, R. E. I. Schropp, H. A. Atwater, and A. Polman, Nano Lett. **11**(10), 4239 (2011).
[74]J. Bhattacharya, N. Chakravarty, S. Pattnaik, W. Dennis Slafer, R. Biswas, and V. L. Dalal, Appl. Phys. Lett. **99**(13), 131114 (2011).
[75]C. Battaglia, C.-M. Hsu, K. Söderström, J. Escarré, F.-J. Haug, M. Charrière, M. Boccard, M. Despeisse, D. T. L. Alexander, M. Cantoni, Y. Cui, and C. Ballif, ACS Nano **6**(3), 2790 (2012).
[76]O. Isabella, F. Moll, J. Krč, and M. Zeman, Phys. Status Solidi A **207**(3), 642 (2010).
[77]C. Haase and H. Stiebig, Prog. Photovoltaics **14**(7), 629 (2006).
[78]M. G. Moharam and T. K. Gaylord, J. Opt. Soc. Am. **72**(10), 1385 (1982).
[79]M. G. Moharam, E. B. Grann, D. A. Pommet, and T. K. Gaylord, J. Opt. Soc. Am. A **12**(5), 1068 (1995).
[80]Z. Yu, A. Raman, and S. Fan, Opt. Express **18**(S3), A366 (2010).
[81]T. Clausnitzer, T. Kämpfe, E. B. Kley, A. Tünnermann, U. Peschel, A. V. Tishchenko, and O. Parriaux, Opt. Express **13**(26), 10448 (2005).
[82]A. V. Tishchenko, Opt. Quantum Electron. **37**, 309 (2005).
[83]K. R. Catchpole, J. Appl. Phys. **102**(1), 013102 (2007).

[84]M. Born and E. Wolf, *Principles of Optics*, 7th ed. (Cambridge University press, 2001).
[85]J. W. Goodman, *Introduction to Fourier optics*, 3rd ed. (McGraw-Hill, 1996).
[86]S. Sinzinger and M. Testorf, Appl. Opt. **34**(26), 5970 (1995).
[87]S. Mokkapati *et al*., J. Phys. D: Appl. Phys. **44**(5), 055103 (2011).
[88]Z. Yu, A. Raman, and S. Fan, Proc. Natl. Acad. Sci. U. S. Am. **107**, 17491 (2010).
[89]S. Basu Mallick, M. Agrawal, and P. Peumans, Opt. Express **18**(6), 5691 (2010).
[90]I. Tobias, A. Luque, and A. Marti, J. Appl. Phys. **104**(3), 034502 (2008).
[91]P. Campbell and M. A. Green, IEEE Trans. Electron Devices **ED-33**(2), 234 (1986).
[92]A. Luque, Sol. Energy Mater. **23**, 152 (1991).
[93]R. W. Boyd, *Radiometry and the Detection of Optical Radiation* (Wiley, New York, 1983).
[94]I. Tobias, J. Appl. Phys. **104**, 034502 (2008).
[95]Z. Yu and S. Fan, *Angular Constraint on Light-Trapping Absorption Enhancement in Solar Cells* (AIP, 2011), p. 011106.
[96]Z. Yu, A. Raman, and S. Fan, Proc. Natl. Acad. Sci. U.S.A. **107**(41), 17491 (2010).
[97]X. Sheng, S. G. Johnson, J. Michel, and L. C. Kimmerling, Opt. Express **19**, A841 (2011).
[98]F. Llopis and I. Tobías, Sol. Energy Mater. Sol. Cells **87**(1–4), 481 (2005).
[99]C. Heine and R. H. Morf, Appl. Opt. **34**(14), 2476 (1995).
[100]S. Eon Han and G. Chen, Nano Lett. **10**(11), 4692 (2011).
[101]H. R. Stuart and D. G. Hall, *Absorption Enhancement in Silicon-on-Insulator Waveguides Using Metal Island Films* (AIP, 1996), p. 2327.
[102]D. M. Schaadt, B. Feng, and E. T. Yu, Appl. Phys. Lett. **86**(6), 063106 (2005).
[103]D. Derkacs, S. H. Lim, P. Matheu, W. Mar, and E. T. Yu, Appl. Phys. Lett. **89**(9), 093103 (2006).
[104]P. Matheu, S. H. Lim, D. Derkacs, C. McPheeters, and E. T. Yu, Appl. Phys. Lett. **93**(11), 113108 (2008).
[105]S. Pillai, K. R. Catchpole, T. Trupke, and M. A. Green, J. Appl. Phys. **101**(9), 093105 (2007).
[106]N. Keisuke, T. Katsuaki, and A. Atwater Harry, Appl. Phys. Lett. **93**(12), 121904 (2008).
[107]D. Derkacs, W. V. Chen, P. M. Matheu, S. H. Lim, P. K. L. Yu, and E. T. Yu, Appl. Phys. Lett. **93**(9), 091107 (2008).
[108]B. P. Rand, P. Peumans, and S. R. Forrest, J. Appl. Phys. **96**(12), 7519 (2004).
[109]K. Seok-Soon, N. Seok-In, J. Jang, K. Dong-Yu, and N. Yoon-Chae, Appl. Phys. Lett. **93**(7), 073307 (2008).
[110]C. Hagglund, M. Zach, G. Petersson, and B. Kasemo, Appl. Phys. Lett. **92**(5), 053110 (2008).
[111]T. Kume, S. Hayashi, H. Ohkuma, and K. Yamamoto, Jpn. J. Appl. Phys., Part 1 **34**(12A), 6448 (1995).
[112]R. B. Konda, R. Mundle, H. Mustafa, O. Bamiduro, A. K. Pradhan, U. N. Roy, Y. Cui, and A. Burger, Appl. Phys. Lett. **91**(19), 191111 (2007).
[113]M. Kirkengen, J. Bergli, and Y. M. Galperin, J. Appl. Phys. **102**(9), 093713 (2007).
[114]V. E. Ferry, L. A. Sweatlock, D. Pacifici, and H. A. Atwater, Nano Lett. **8**(12), 4391 (2008).
[115]K. R. Catchpole and A. Polman, Opt. Express **16**(26), 21793 (2008).
[116]H. A. Atwater and A. Polman, Nature Mater. **9**(3), 205 (2010).
[117]V. E. Ferry, J. N. Munday, and H. A. Atwater, Adv. Mater. **22**(43), 4794 (2010).
[118]L. Tsakalakos, *Nanotechnology for Photovoltaics*, (CRC, MA, 2010), p. 49.
[119]C. Battaglia, K. Soderstrom, J. Escarre, F.-J. Haug, D. Domine, P. Cuony, M. Boccard, G. Bugnon, C. Denizot, M. Despeisse, A. Feltrin, and C. Ballif, Appl. Phys. Lett. **96**(21), 213504 (2010).
[120]C. Rockstuhl, S. Fahr, K. Bittkau, T. Beckers, R. Carius, F. J. Haug, T. Söderström, C. Ballif, and F. Lederer, Opt. Express **18**(S3), A335 (2010).
[121]Y. Tawada, H. Yamagishi, and K. Yamamoto, Sol. Energy Mater. Sol. Cells **78**(1–4), 647 (2003).
[122]K. Yamamoto, M. Yoshimi, Y. Tawada, S. Fukuda, T. Sawada, T. Meguro, H. Takata, T. Suezaki, Y. Koi, K. Hayashi, T. Suzuki, M. Ichikawa, and A. Nakajima, Sol. Energy Mater. Sol. Cells **74**(1–4), 449 (2002).
[123]M. A. Green, K. Emery, Y. Hishikawa, and W. Warta, Prog. Photovoltaics **19**(1), 84 (2011).
[124]S. Fahr, C. Rockstuhl, and F. Lederer, Appl. Phys. Lett. **92**(17), 171114 (2008).
[125]C. Rockstuhl, S. Fahr, F. Lederer, K. Bittkau, T. Beckers, and R. Carius, Appl. Phys. Lett. **93**(6), 061105 (2008).
[126]N. Bonod and E. Popov, Opt. Lett. **33**, 2398 (2008).
[127]R. H. Franken, R. L. Stolk, H. Li, C. H. M. van der Werf, J. K. Rath, and R. E. I. Schropp, J. Appl. Phys. **102**(1), 014503 (2007).
[128]M. D. Kelzenberg, S. W. Boettcher, J. A. Petykiewicz, D. B. Turner-Evans, M. C. Putnam, E. L. Warren, J. M. Spurgeon, R. M. Briggs, N. S. Lewis, and H. A. Atwater, Nat. Mater. **9**, 239 (2010).
[129]E. Garnett and P. Yang, Nano Lett. **10**, 1082 (2010).
[130]O. L. Muskens, J. Gómez Rivas, R. E. Algra, E. P. A. M. Bakkers, and A. Lagendijk, Nano Lett. **8**(9), 2638 (2008).
[131]B. C. P. Sturmberg, K. B. Dossou, L. C. Botten, A. A. Asatryan, C. G. Poulton, C. Martijn de Sterke, and R. C. McPhedran, Opt. Express **19**(S5), A1067 (2011).
[132]B. M. Kayes, H. A. Atwater, and N. S. Lewis, J. Appl. Phys. **97**, 114302 (2005).
[133]M. C. Putnam, D. B. Turner-Evans, M. D. Kelzenberg, S. W. Boettcher, N. S. Lewis, and H. A. Atwater, Appl. Phys. Lett. **95**(16), 163116 (2009).
[134]K. E. Plass, M. A. Filler, J. M. Spurgeon, B. M. Kayes, S. Maldonado, B. S. Brunschwig, H. A. Atwater, and N. S. Lewis, Adv. Mater. **21**, 325 (2009).
[135]R. Kapadia, Z. Fan, and A. Javey, Appl. Phys. Lett. **96**, 103116 (2010).
[136]B. Tian, X. Zheng, T. J. Kempa, Y. Fang, N. Yu, G. Yu, J. Huang, and C. M. Lieber, Nature (London) **449**(7164), 885 (2007).
[137]V. Sivakov, G. Andrä, A. Gawlik, A. Berger, J. Plentz, F. Falk, and S. H. Christiansen, Nano Lett. **9**(4), 1549 (2009).
[138]Y. Dong, B. Tian, T. J. Kempa, and C. M. Lieber, Nano Lett. **9**(5), 2183 (2009).
[139]Y. B. Tang, Z. H. Chen, H. S. Song, C. S. Lee, H. T. Cong, H. M. Cheng, W. J. Zhang, I. Bello, and S. T. Lee, Nano Lett. **8**(12), 4191 (2008).
[140]M. J. Stocks, A. Cuevas, and A. W. Blakers, Prog. Photovoltaics **4**, 35 (1996).
[141]K. R. Catchpole, S. Mokkapati, and F. Beck, J. Appl. Phys. **109**, 084519 (2011).
[142]H. R. Stuart and D. G. Hall, J. Opt. Soc. Am. A **14**(11), 3001 (1997).
[143]D. M. Callahan, J. N. Munday, and H. A. Atwater, Nano Lett. **12**, 214 (2011).
[144]J. N. Munday, D. M. Callahan, and H. A. Atwater, Appl. Phys. Lett. **100**, 121121 (2012).
[145]M. A. Green, Prog. Photovoltaics **19**, 473 (2011).
[146]E. A. Schiff, J. Appl. Phys. **110**(10), 104501 (2011).